

NEURODEGENERATIVE DISEASES

Poly(ADP-ribose) promotes toxicity of C9ORF72 arginine-rich dipeptide repeat proteins

Junli Gao^{1†}, Quinlan T. Mewborne^{1†}, Amandeep Girdhar², Udit Sheth¹, Alyssa N. Coyne^{3,4}, Ritika Punathil¹, Bong Gu Kang³, Morgan Dasovich^{5,6}, Austin Veire¹, Mariely DeJesus Hernandez¹, Shuaichen Liu⁵, Zheng Shi⁷, Ruxandra Dafinca⁸, Elise Fouquerel², Kevin Talbot⁸, Tae-In Kam³, Yong-Jie Zhang¹, Dennis Dickson¹, Leonard Petrucelli^{1,9}, Marka van Blitterswijk¹, Lin Guo², Ted M. Dawson^{3,10,11}, Valina L. Dawson^{3,10,11}, Anthony K. L. Leung^{5,12,13,14}, Thomas E. Lloyd^{3,11}, Tania F. Gendron^{1,9}, Jeffrey D. Rothstein^{3,4,11*}, Ke Zhang^{1,9,15*}

Copyright © 2022 The Authors, some rights reserved; exclusive licensee American Association for the Advancement of Science. No claim to original U.S. Government Works

Arginine-rich dipeptide repeat proteins (R-DPRs), abnormal translational products of a GGGGCC hexanucleotide repeat expansion in *C9ORF72*, play a critical role in *C9ORF72*-related amyotrophic lateral sclerosis (ALS) and frontotemporal dementia (FTD), the most common genetic form of the disorders (c9ALS/FTD). R-DPRs form liquid condensates in vitro, induce stress granule formation in cultured cells, aggregate, and sometimes coaggregate with TDP-43 in postmortem tissue from patients with c9ALS/FTD. However, how these processes are regulated is unclear. Here, we show that loss of poly(ADP-ribose) (PAR) suppresses neurodegeneration in c9ALS/FTD fly models and neurons differentiated from patient-derived induced pluripotent stem cells. Mechanistically, PAR induces R-DPR condensation and promotes R-DPR-induced stress granule formation and TDP-43 aggregation. Moreover, PAR associates with insoluble R-DPR and TDP-43 in postmortem tissue from patients. These findings identified PAR as a promoter of R-DPR toxicity and thus a potential target for treating c9ALS/FTD.

INTRODUCTION

A GGGGCC (G_4C_2) hexanucleotide repeat expansion in the *C9ORF72* gene is the most common genetic cause of amyotrophic lateral sclerosis (ALS) and frontotemporal dementia (FTD) (1, 2). Two unique pathological hallmarks of *C9ORF72*-mediated ALS and frontotemporal lobar degeneration (FTLD), the neuropathological diagnosis of FTD, are foci of repeat-containing transcripts and aggregation of abnormal translation products of these transcripts, dipeptide repeat proteins (DPRs) (3–8). Among the five DPR species—namely, poly(glycine-arginine) (GR), poly(glycine-alanine) (GA), poly(glycine-proline) (GP), poly(proline-alanine) (PA), and poly(proline-arginine) (PR)—the arginine-rich DPRs (R-DPRs) poly(GR) and poly(PR) are particularly toxic when overexpressed in cell or animal models (9–16). However, what regulates R-DPR aggregation is unclear.

Stress granules (SGs) are cytoplasmic RNA/protein condensates assembled in cells upon diverse cellular stressors (17). Upon stress, ribosomes disassemble, and mRNAs are embedded into SGs enriched in RNA binding proteins, whose liquid-liquid phase separation (LLPS) mediates SG assembly (18–20). Normally, SGs are dynamic and can disassemble when stress is removed (17, 21); however, SGs with aberrant dynamics are related to the aggregation of SG proteins TDP-43, Fused in sarcoma (FUS), and other heterogeneous nuclear ribonucleoproteins (hnRNPs), which is a pathological hallmark of ALS and FTD, including c9ALS/FTD (22–25).

Previous studies identified a critical role of SGs in R-DPR-mediated cytotoxicity. R-DPRs interact with many SG proteins, and their overexpression causes the formation of aberrant, poorly dynamic SGs in cells without additional stress (11, 14, 26). Furthermore, chemically synthesized R-DPRs can undergo LLPS, recruit SG proteins, and cause SG protein precipitation when added into cell lysates (26). In agreement with these data, poly(GR) localizes to SGs in cells, promotes the aggregation of recombinant TDP-43 in vitro, and coaggregates with TDP-43 and the SG protein eIF3 η in postmortem tissue from patients with c9ALS/FTD (27). We have previously found that inhibiting SG assembly by genetic or pharmacological approaches suppresses R-DPR-induced cytotoxicity or neurodegeneration in cellular or animal models (14). Together, these findings suggest that R-DPRs promote aberrant SG formation and protein aggregation, which contributes to neurodegeneration. However, how these processes are regulated is unclear.

Poly(ADP-ribose) (PAR) is a highly dynamic polymer that post-translationally modifies proteins, a process known as PARylation. It is tightly regulated by PAR polymerases (PARPs) and PAR glycohydrolase (PARG), which synthesizes and degrades PAR, respectively (28). As a posttranslational modification, PAR plays an essential role in cellular physiology, including SG assembly. Many SG proteins are PARylated or bind to PAR (29, 30). However, elevated PAR can be toxic. For example, PARP1 hyperactivation can induce a special

¹Department of Neuroscience, Mayo Clinic, Jacksonville, FL 32224, USA. ²Department of Biochemistry and Molecular Biology, Thomas Jefferson University, Philadelphia, PA 19107, USA. ³Department of Neurology, Johns Hopkins University, School of Medicine, Baltimore, MD 21205, USA. ⁴Brain Science Institute, Johns Hopkins University, School of Medicine, Baltimore, MD 21205, USA. ⁵Department of Biochemistry and Molecular Biology, Bloomberg School of Public Health, Johns Hopkins University, Baltimore, MD 21205, USA. ⁶Department of Chemistry, Krieger School of Arts and Sciences, Johns Hopkins University, Baltimore, MD 21218, USA. ⁷Department of Chemistry and Chemical Biology, Rutgers University, Piscataway, NJ 08854, USA. ⁸Nuffield Department of Clinical Neurosciences, John Radcliffe Hospital, University of Oxford, Oxford OX3 9DU, UK. ⁹Neuroscience Graduate Program, Mayo Clinic Graduate School of Biomedical Sciences, Jacksonville, FL 32224, USA. ¹⁰Neuroregeneration and Stem Cell Programs, Institute for Cell Engineering, Johns Hopkins University, School of Medicine, Baltimore, MD 21205, USA. ¹¹Department of Neuroscience, Johns Hopkins University, School of Medicine, Baltimore, MD 21205, USA. ¹²McKusick-Nathans Department of Genetic Medicine, Johns Hopkins University School of Medicine, Baltimore, MD 21205, USA. ¹³Department of Oncology, Johns Hopkins University School of Medicine, Baltimore, MD 21205, USA. ¹⁴Department of Molecular Biology and Genetics, Johns Hopkins University School of Medicine, Baltimore, MD 21205, USA. ¹⁵Institute of Neurological Diseases, Shenzhen Bay Laboratory, Shenzhen, Guangdong, 518132, China.

*Corresponding author. Email: ke.zhang@szbl.ac.cn (K.Z.); jrothstein@jhmi.edu (J.D.R.)

†The authors contributed equally to this work.

type of programmed cell death called parthanatos, whereas loss of PARG, respectively, causes neurodegeneration or embryonic lethality in *Drosophila* or mice (31–33). In c9ALS/FTD, elevated nuclear PAR was reported in neurons from patients (34), but whether and how PAR relates to c9ALS/FTD pathogenesis is unclear.

Here, we show that loss of PARP1 (fly homolog: Parp) function suppresses R-DPR aggregation and neurodegeneration in c9ALS/FTD fly models and/or neurons differentiated from patient-derived induced pluripotent stem cells (iPSCs). Mechanistically, PAR interacts with R-DPRs, induces their condensation, and enhances their ability to induce aberrant SG formation and TDP-43 aggregation. Furthermore, PAR associates with detergent-insoluble poly(GR) and pathologic TDP-43 in frontal cortex tissue from patients with c9ALS/FTD. Together, our data support a role of PAR in promoting R-DPR toxicity and suggest that it might be a therapeutic target.

RESULTS

Loss of Parp/PARP1 function suppresses neurodegeneration in c9ALS/FTD models

In a previously published screen, we identified 102 genes whose RNA interference (RNAi) strongly or moderately suppress eye degeneration in a *Drosophila* model of c9ALS/FTD, in which flies express 30 repeats of G_4C_2 [(G_4C_2)₃₀] using the upstream activated sequence (UAS)/Galactin 4 (GAL4) system (35) under the control of glass multiple reporter (GMR)–GAL4 (36). Comparing these results to RNAi screen results from independent studies using other fly models of c9ALS/FTD (11, 37), we found that *parp*, the fly homolog of human PARP1, is one of the only four genes identified from more than one screen (fig. S1A).

To verify that *parp* RNAi suppresses neurodegeneration in fly models of c9ALS/FTD, we tested two independent *parp* RNAi lines and showed that they both suppressed eye degeneration in the (G_4C_2)₃₀ model (Fig. 1A). Furthermore, overexpressing PARG, which decreased PAR (31, 32), also suppressed eye degeneration in the (G_4C_2)₃₀ flies (Fig. 1A). Next, we tested whether *parp* RNAi suppresses eye degeneration in other c9ALS/FTD fly models. Among all five DPR species, only the R-DPRs, poly(GR) and poly(PR), cause eye degeneration in flies (9, 11). *Parp* RNAi suppressed eye degeneration in flies expressing 36 repeats of GR or PR [(GR)₃₆ or (PR)₃₆] using alternative non- G_4C_2 repeat codons under the control of GMR–GAL4

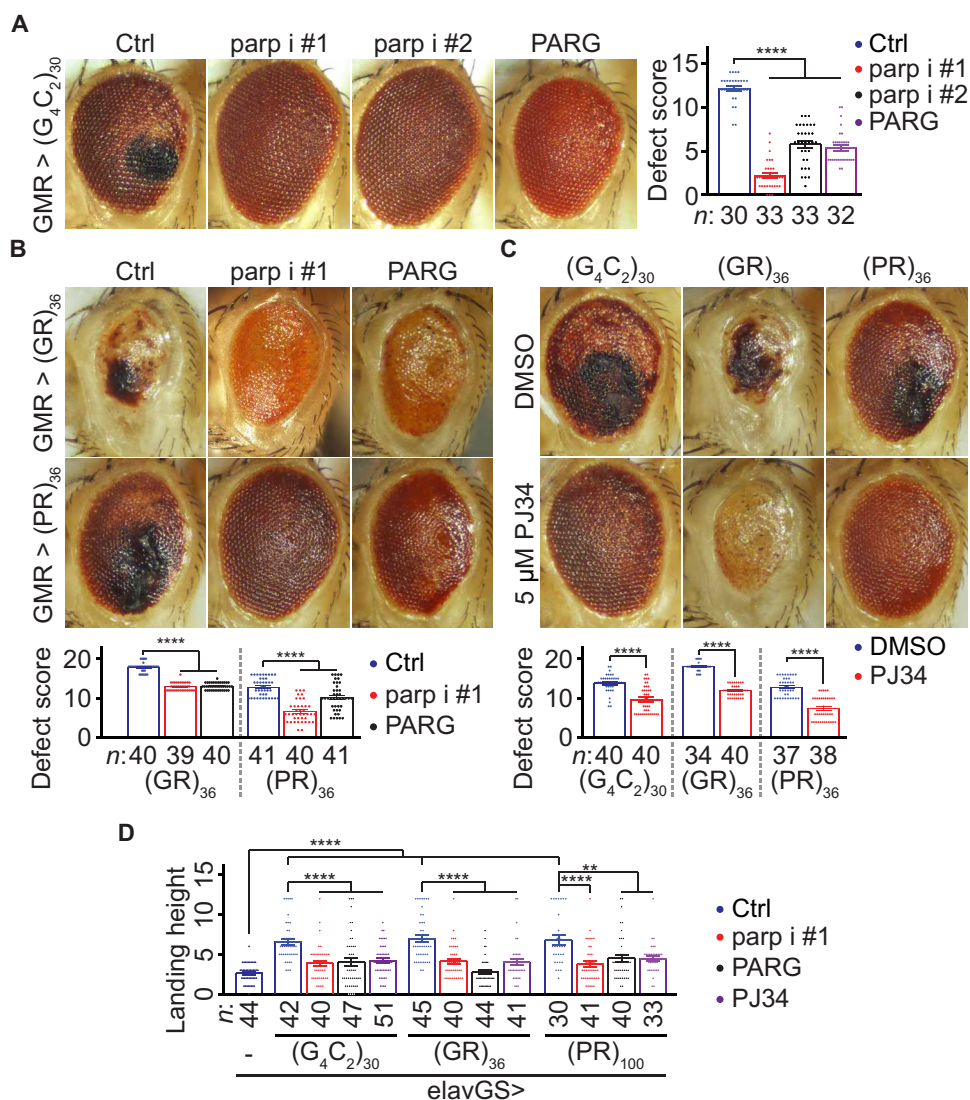


Fig. 1. Loss of Parp/PARP1 function suppresses neurodegeneration in fly models of c9ALS/FTD. (A) Fly eyes expressing (G_4C_2)₃₀, under the control of GMR–GAL4, with or without *parp* RNAi (*parp* i) or PARG cDNA. Right: Fly eye defects were scored using a published method (79). Briefly, points were added if there was a complete loss of interommatidial bristles, necrotic patches, retinal collapse, loss of ommatidial structure, and/or depigmentation of the eye. (B) Fly eyes expressing (GR)₃₆ or (PR)₃₆ with or without *parp* RNAi or PARG cDNA. Quantification of the eye scores at the bottom. (C) Eyes of flies expressing (G_4C_2)₃₀, (GR)₃₆, or (PR)₃₆ and fed with DMSO or PJ34. Quantified at the bottom. (D) Flight assays (see Materials and Methods). One-way analysis of variance (ANOVA) with Dunnett's tests (A, B, and D) and Student's *t* tests (C). ***P* < 0.01 and *****P* < 0.0001. Means ± SEM.

(Fig. 1B) without decreasing R-DPR (fig. S1B). Furthermore, PARG overexpression (Fig. 1B) or feeding (G_4C_2)₃₀, (GR)₃₆, or (PR)₃₆ flies with PJ34, a fly Parp and human PARP1/2 inhibitor (38), also suppressed eye degeneration (Fig. 1C). Together, our data suggest that decreasing PAR suppresses eye degeneration in multiple fly models of c9ALS/FTD.

Next, we tested whether decreasing PAR suppresses locomotion defects in fly models of c9ALS/FTD. Previously, we showed that, using a gene-switch system (*elavGS*), pan-neuronal expression of (G_4C_2)₃₀ impairs flight of aged flies (36). Here, we show that using alternative codons, pan-neuronal expression of (GR)₃₆ and 100 repeats of PR [(PR)₁₀₀], also caused flight defects in aged flies (Fig. 1D).

Furthermore, *parp* RNAi, PARG overexpression, or PJ34 feeding suppressed these defects, suggesting that down-regulating PAR mitigates locomotion defects in multiple fly models of c9ALS/FTD.

To validate our findings above in a patient-derived model, we used four c9ALS/FTD iPSC-derived neuron (iPSN) lines along with three age- and sex-matched control lines and an isogenic control line (fig. S2A). We used a previously established protocol to generate iPSNs expressing several neuronal markers, including ISL1, NK6 Homeobox 1 (NKX6.1), SMI32, and Tubulin Beta 3 Class III (TUBB3), 32 days after the onset of differentiation (39–41). A common neuronal defect implicated in ALS/FTD, including c9ALS/FTD, is hypersensitivity to glutamate-induced excitotoxicity (2, 7, 42, 43). Using propidium iodide (PI) staining to label dead neurons, we previously showed that a 4-hour treatment of c9ALS/FTD iPSNs with 10 μ M glutamate caused more cell death compared to control iPSNs (39).

Here, we verified these findings (Fig. 2, A and B, and fig. S2C) and further showed that a 5-day pretreatment with the PARP1/2 inhibitors niraparib or veliparib reduced PAR (fig. S2B) and glutamate-induced neuronal death (Fig. 2, A and B, and fig. S2C). Furthermore, PARP1 RNAi or PARG overexpression also suppressed glutamate-induced neuronal death in c9ALS/FTD iPSN line #1 (fig. S2D), suggesting that decreasing PAR could reduce neurotoxicity in c9ALS/FTD iPSNs. Consistent with these data, c9ALS/FTD iPSNs exhibited elevated PAR compared to the control iPSNs (Fig. 2, C and D).

Previous studies showed that treating U-2 osteosarcoma (OS) cells with chemically synthesized peptides of 20 repeats of GR or PR [(GR)₂₀ or (PR)₂₀] caused cytotoxicity, as measured by the enzymatic MTT assay (10). To directly assess R-DPR toxicity in iPSNs, we treated a control iPSN line (Ctrl#1) with (GR)₂₀ or (PR)₂₀ and evaluated cytotoxicity using an enzymatic assay that measures the release of lactate dehydrogenase (LDH) from neurons due to damaged plasma membranes (44). As shown in Fig. 2E, a 2-day treatment with 5 μ M (GR)₂₀ or (PR)₂₀, but not 20 repeats of GP, [(GP)₂₀], a nontoxic DPR (9, 45), enhanced LDH release in these iPSNs. Furthermore, a 1-day pretreatment with 5 μ M niraparib or veliparib reduced (GR)₂₀- or (PR)₂₀-induced PAR up-regulation and LDH release without affecting intracellular poly(GR) or poly(PR) (Fig. 2E and fig. S2, E to G). In addition, adding (GR)₂₀ reversed niraparib- and veliparib-mediated suppression of glutamate-induced neuronal death in c9ALS/FTD iPSN line #1 (fig. S2H). In summary, our data suggest that down-regulating PAR suppresses neuronal defects in both fly and iPSN models of c9ALS/FTD.

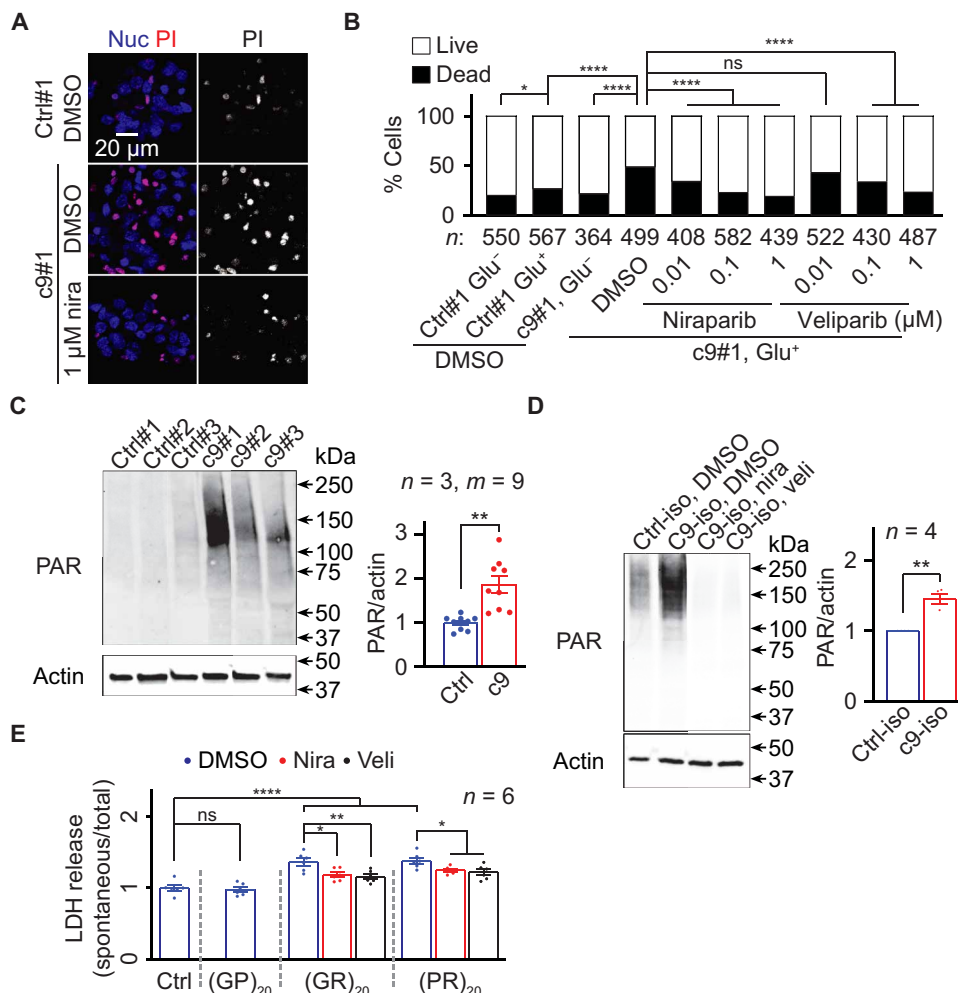


Fig. 2. Loss of Parp/PARP1 function suppresses neurodegeneration in c9ALS/FTD iPSNs. (A) Control line #1 (Ctrl#1) or c9ALS/FTD line #1 (c9#1) iPSNs pretreated with DMSO or niraparib (nira), treated with glutamate, and stained with propidium iodide (PI; red) and NucBlue (Nuc; blue). (B) Quantification of glutamate toxicity assays on Ctrl#1 and c9#1 iPSNs pretreated with DMSO, nira, or veliparib (veli). For each condition, three visual frames were imaged, and total numbers of cells were counted. The experiments were biologically replicated twice. (C and D) Immunoblots of lysates from three age- and sex-matched pairs (C) and an isogenic pair (D) of Ctrl and c9 iPSNs. In (C), three replicates of three iPSN pairs ($n = 3$, total $m = 9$ data points) were used for statistical analyses. (E) LDH assays on Ctrl#1 iPSNs pretreated with DMSO or 5 μ M nira or veli and treated with 10 μ M DPRs. χ^2 tests (B), Student's t tests (C and D), and one-way ANOVA with Dunnett's tests (E). ns, not significant. $*P < 0.05$, $**P < 0.01$, and $****P < 0.0001$. Means \pm SEM.

PAR binds to R-DPRs and induces their condensation in vitro

PAR was shown to bind to TDP-43, FUS, hnRNP A1, α -synuclein, and several other proteins to promote their condensation via either LLPS or aggregation and to contribute to TDP-43 and α -synuclein toxicity (30, 46–55). As R-DPR aggregation is a pathological hallmark of c9ALS/FTD (3–6, 8), we hypothesized that PAR could bind R-DPRs, thus promoting their condensation. PAR is negatively charged, and many PAR-binding protein domains are enriched in positively charged amino acids such as arginine (50, 56). To test whether PAR binds to R-DPRs, we first performed co-immunoprecipitation (co-IP) assays on human embryonic kidney (HEK) 293T cells transiently overexpressing green fluorescent protein (GFP)-tagged 50 repeats of DPRs [(DPR)₅₀-GFP] using alternative codons. To inhibit ectopic PARP and

PARG activation caused by cell lysis, which can skew co-IP results (56, 57), we added PJ34 and the PARG inhibitor PDD00017273 (PARGin) to our cell lysis and IP buffers. As shown in Fig. 3A, (GR)₅₀- and (PR)₅₀-GFP coimmunoprecipitated with PAR, suggesting that PAR can associate with R-DPRs in cells. Ribonuclease treatment did not reduce this association (fig. S3A), suggesting that the effect was not due to RNA-mediated mechanisms. Compared to the control and other DPRs, (GR)₂₀ and (PR)₂₀ showed stronger binding to chemically synthesized PAR in dot blot binding assays (Fig. 3B and fig. S3B), suggesting that PAR directly interacts with R-DPRs in vitro.

RNA, which is negatively charged and structurally similar to PAR, can promote R-DPR LLPS in a phosphate buffer (26). Thus, we tested whether synthetic PAR could promote R-DPR LLPS in the same buffer. As shown by differential interference contrast (DIC) images in fig. S3 (C and D), PAR, but not mono(ADP-ribose) (MAR), caused (GR)₂₀ or (PR)₂₀ to phase separate into condensates without crowding agents. These condensates were about 1 to 2 μm in diameter. To better study these condensates, we labeled (GR)₂₀ or (PR)₂₀ with the 5-carboxytetramethylrhodamine (TAMRA) fluorophore. Similar to unlabeled R-DPRs, PAR, but not MAR, caused TAMRA-R-DPRs to phase separate into condensates without crowding agents (Fig. 3C).

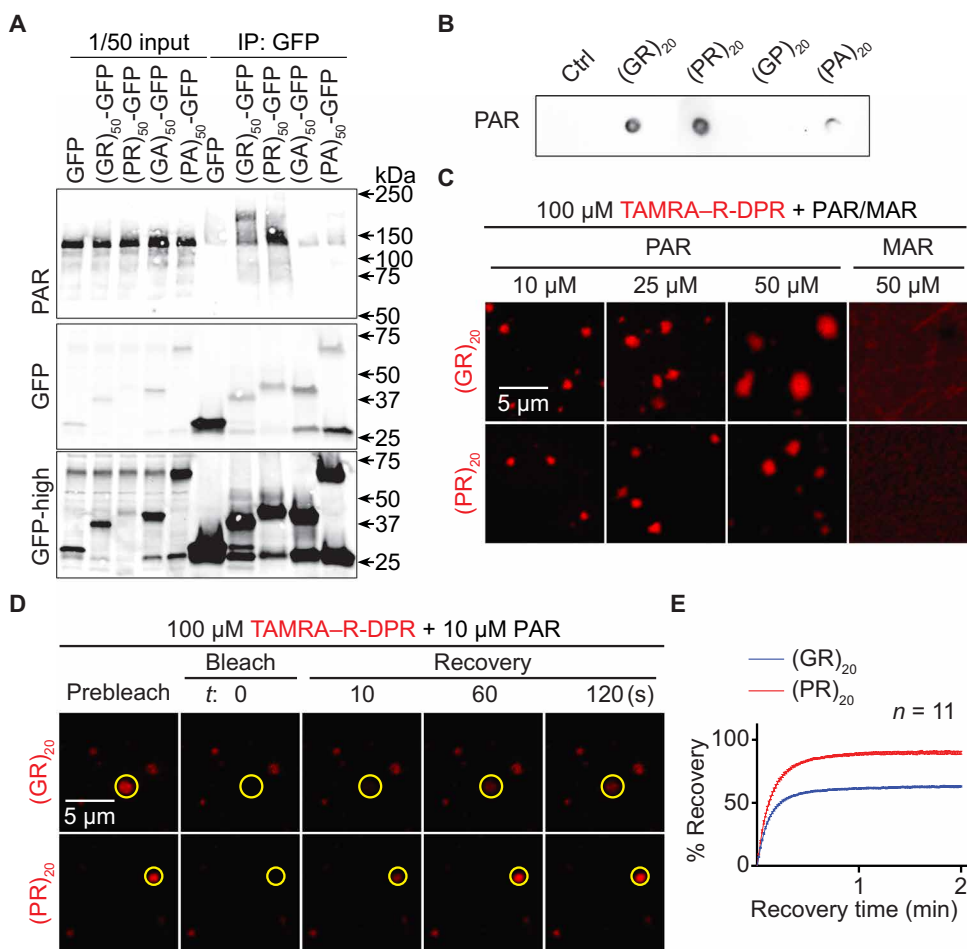


Fig. 3. PAR induces R-DPR condensation in vitro. (A) Co-IP of PAR and DPRs in HEK293T cells. (B) Dot blot binding assays of PAR and DPRs. (C) TAMRA-R-DPR (red) mixed with PAR (10 to 50 μM) or MAR. (D and E) FRAP assays on PAR and TAMRA-R-DPR condensates. Yellow circles indicate bleached and analyzed areas. Total R-DPRs (1 μM) were labeled. Buffer for (C to E): 61.5 mM K₂HPO₄ and 38.5 mM KH₂PO₄.

Using fluorescent recovery after photobleaching (FRAP) assays, we photobleached individual TAMRA-R-DPR condensates and found that the fluorescence was partially recovered, suggesting that a fraction of TAMRA-R-DPR was mobile (Fig. 3, D and E). To study the relationship of R-DPRs and PAR in these condensates, we labeled PAR with the Cy5 fluorophore using a previously published method (58). Of interest, we observed Cy5 emission excited by lasers with a TAMRA excitation wavelength (fig. S3, E and F), suggesting Förster resonant energy transfer (FRET) from TAMRA-(GR)₂₀ or TAMRA-(PR)₂₀ to PAR-Cy5. We verified the FRET with the acceptor photobleaching method (59), showing that photobleaching the Cy5 signal restored TAMRA intensity (fig. S3, G and H). Because FRET typically occurs between molecules within a 10-nm distance range to allow bimolecular interactions (59), these data confirmed that PAR directly interacted with R-DPRs. Together, our data suggest that PAR binds to R-DPRs and promotes their condensation in vitro.

Loss of PARP1 activity suppresses R-DPR-induced SG formation

SGs play a critical role in R-DPR toxicity (11, 13, 14, 26). Overexpression of R-DPRs induces spontaneous formation of aberrant SGs in cells (11, 14, 26), whereas inhibiting SG assembly by genetic or pharmacological approaches suppresses R-DPR-mediated cellular defects (14). Since PARP1 inhibitors suppress or delay SG assembly induced by DNA damage or arsenite stress (29, 30), we hypothesized that loss of PARP1 activity could mitigate R-DPR-induced SG formation.

To study R-DPR-induced SG formation, we stained HEK293T cells overexpressing (GR)₅₀- or (PR)₅₀-GFP for 8, 24, or 48 hours with the SG markers Ras GTPase-activating protein-binding protein 1 (G3BP1) and Ataxin-2. We did not observe SGs after 8 hours of overexpression (~150 cells counted); however, about 30 to 40% of GFP-expressing cells exhibited SGs after 24 or 48 hours (Fig. 4, A and B), suggesting that R-DPRs induced SG formation in a relatively slow manner compared to arsenite, which induces SG formation within an hour. Consistent with previous studies (11), (GR)₅₀-GFP, but not (PR)₅₀-GFP, localized to SGs (Fig. 4A and fig. S4A).

Next, we tested whether PARP1 knockout (KO) could mitigate R-DPR-induced SG formation. As shown in Fig. 4 (A and B) and fig. S4B, PARP1 KO decreased the percentage of cells with SGs after 24 or 48 hours of (GR)₅₀- or (PR)₅₀-GFP overexpression. We chose the 24-hour time point for our subsequent analyses. Similar to PARP1 KO, a 2-hour pretreatment of 1 μM niraparib or veliparib decreased the percent of

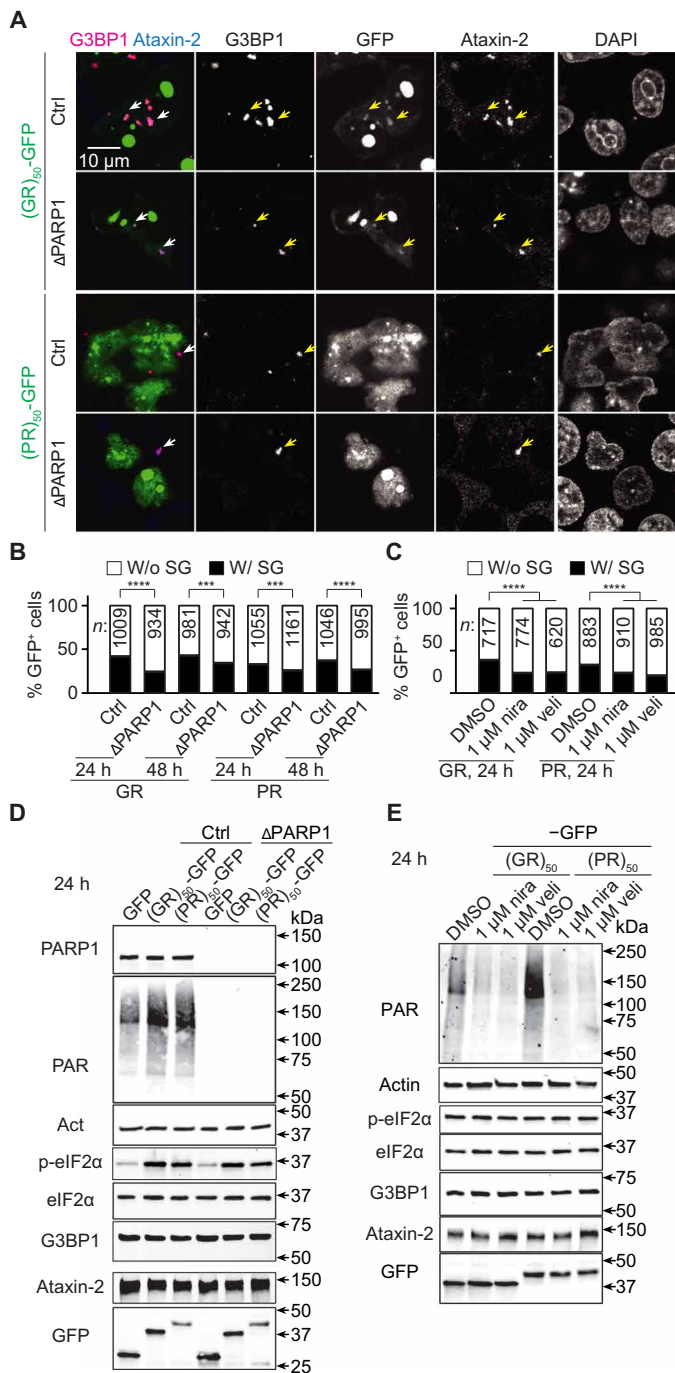


Fig. 4. Loss of PARP1 activity suppresses R-DPR-induced SG formation. (A) Control (Ctrl) or PARP1 KO (Δ PARP1) HEK293T cells transfected with R-DPR-GFP (green) were immunofluorescently stained for G3BP1 (magenta), Ataxin-2 (blue), and DAPI 24 hours after transfection. Arrowheads indicate SGs. Note that $(GR)_{50}$, but not $(PR)_{50}$, localizes to SGs. (B and C) Quantification of R-DPR-GFP-expressing HEK293T cells that exhibit SGs. (B) Control (Ctrl) or PARP1 KO (Δ PARP1) cells. (C) Ctrl cells treated with DMSO, nira, or veli. DMSO or the PARP1 inhibitors were added to the cells 2 hours before transfection and remained in the culture media until fixation or cell lysis. For each condition, 20 to 30 visual fields from three biological replicates were randomly selected and imaged. The total numbers of GFP-positive cells with or without SGs were separately counted. χ^2 tests. $***P < 0.001$ and $****P < 0.0001$. (D and E) Western blots on HEK293T cells overexpressing R-DPR-GFP for 24 hours. (D) Ctrl or Δ PARP1 cells. (E) Ctrl cells treated with DMSO, nira, or veli.

cells with SGs after 24 hours of $(GR)_{50}$ - or $(PR)_{50}$ -GFP overexpression (Fig. 4C). PARP1 KO or PARP inhibitors did not decrease GFP, G3BP1, or Ataxin-2 amounts (Fig. 4, D and E, and fig. S4C). Together, our data suggest that loss of PARP1 activity reduces R-DPR-induced SG formation.

PAR promotes G3BP1 condensation and interaction with poly(GR)

Next, we studied the mechanism responsible for PARP1-mediated SG formation. Previous studies suggested an essential role of eukaryotic Initiation Factor 2 α (eIF2 α) phosphorylation, as an eIF2 α kinase inhibitor or phospho-dead mutation prevents SG formation induced by R-DPR overexpression (14, 26). However, PARP1 KO or inhibitors did not decrease phospho-eIF2 α in cells expressing $(GR)_{50}$ - or $(PR)_{50}$ -GFP (Fig. 4, D and E, and fig. S4C), suggesting that PARP1 does not promote eIF2 α phosphorylation.

SG assembly is mediated by the condensation of SG proteins, among which G3BP1 plays a pivotal role (18–20). Upon RNA binding, G3BP1 undergoes LLPS, which drives SG assembly. Double KO of G3BP1 and its homolog G3BP2 completely suppresses arsenite- or R-DPR-induced SGs, whereas overexpressing G3BP1 alone induces SGs without additional stress (11, 14, 26, 60). Given that PAR is structurally similar to RNA, we hypothesized that it could also promote G3BP1 LLPS, thereby driving SG formation. Consistent with this hypothesis, G3BP1 can be PARylated and bind to PAR (29, 49, 56, 61), and immunofluorescent staining has detected PAR in arsenite-induced SGs (30).

To test this hypothesis, we mixed synthetic PAR with Alexa-488-labeled recombinant G3BP1 (G3BP1-A488). As shown in Fig. 5 (A and B) and fig. S5 (A and B), PAR, but not MAR, caused G3BP1-A488 to phase separate without crowding agents. Using PAR-Cy5, together with FRAP assays, we showed that a fraction of both PAR and G3BP1 in the condensates is mobile (Fig. 5, C and D), suggesting that PAR promotes G3BP1 LLPS.

Compared to chemical stressors, R-DPRs promote SG assembly via an additional mechanism—they directly interact with some SG proteins. Thus, their LLPS can trigger the condensation of these SG proteins (11, 26). Using co-IP followed by mass spectrometry analyses, a prior study identified 196 proteins interacting with $(GR)_{50}$ - or $(PR)_{50}$ -GFP in HEK293T cells, most of which are SG proteins (11). For some of these proteins, including TIA-1, hnRNP A1, and FUS, $(GR)_{20}$ and/or $(PR)_{20}$ have been shown to promote their condensation (11, 26). These mass spectrometry analyses also identified G3BP1 as an R-DPR interactor. Given the importance of G3BP1 in SG assembly, we hypothesized that R-DPRs might also promote its condensation. Furthermore, because PAR binds to R-DPRs, and G3BP1 is PARylated, we hypothesized that PAR could modulate R-DPR/G3BP1 interactions and enhance the ability of R-DPRs to promote G3BP1 condensation.

First, we used Western blot to verify the interaction between R-DPRs and G3BP1. As shown in fig. S5C, $(GR)_{50}$ -GFP, but not $(PR)_{50}$ -GFP, strongly interacted with G3BP1, consistent with the localization of $(GR)_{50}$, but not $(PR)_{50}$, to SGs (11, 14) (Fig. 4A). As such, also given that poly(GR), but not other DPR, inclusions correlate with neurodegeneration and clinicopathological subtypes (16, 62) and that poly(GR), but not poly(PR), coaggregates with SG proteins in vivo (15, 27), we focused on poly(GR) for our subsequent studies. To test whether PAR modulated the interaction of G3BP1 with $(GR)_{50}$ -GFP, we performed co-IP assays either in PARP1 KO cells

Downloaded from https://www.science.org at Thomas Jefferson University on September 15, 2022

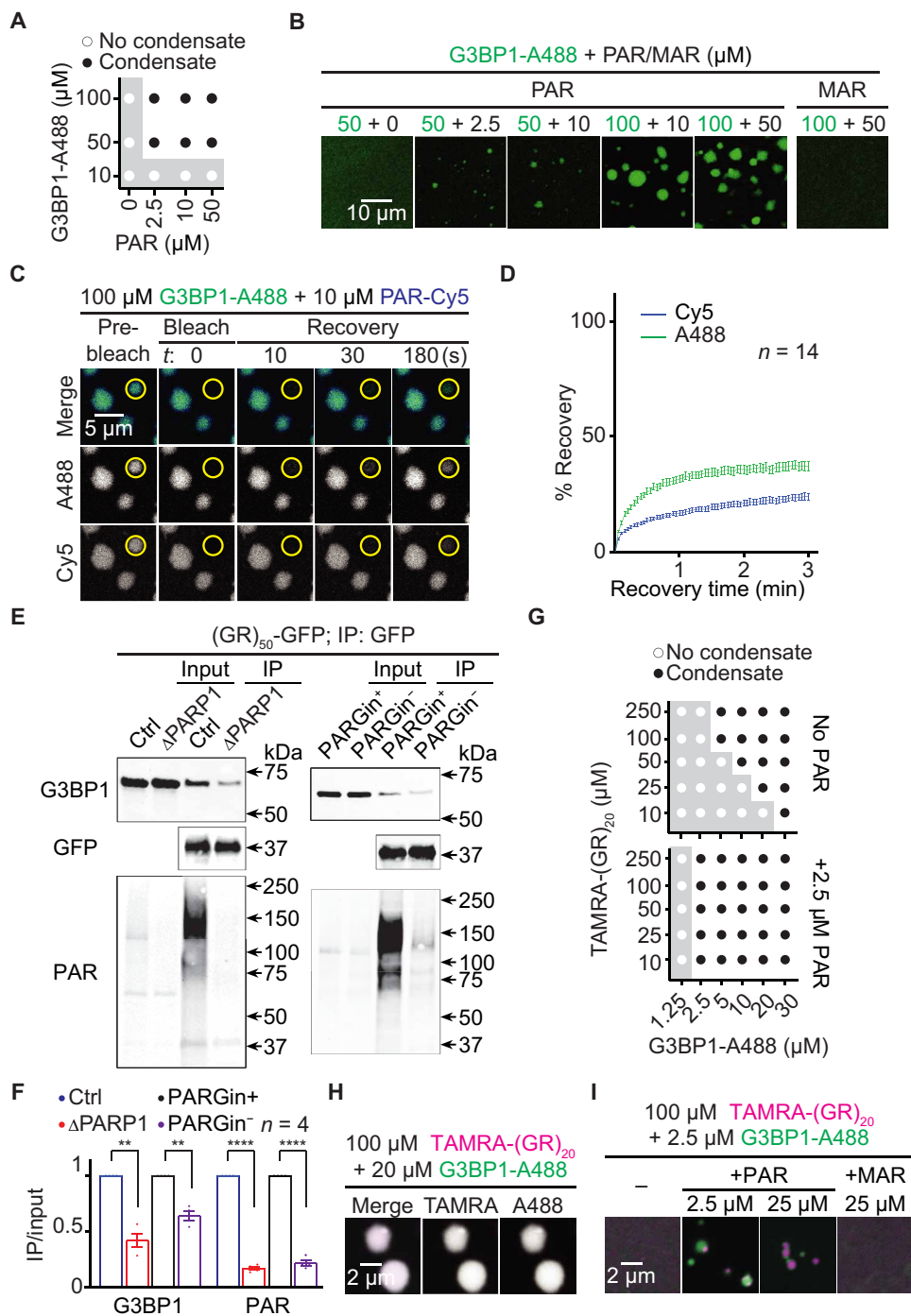


Fig. 5. PAR promotes G3BP1 condensation and interaction with poly(GR). (A) Phase diagram and (B) images of Alexa 488-labeled recombinant G3BP1 (G3BP1-A488; green) mixed with PAR (2.5 to 50 μM MAR equivalents) or 50 μM MAR. (C and D) FRAP assays on G3BP1-A488 (green) and PAR-Cy5 (blue) condensates. Yellow circles indicate bleached and analyzed areas. (E) Co-IP of (GR)₅₀-GFP and endogenous G3BP1 in control (Ctrl) or PARP1 KO (ΔPARP1) HEK293T cells or in Ctrl HEK293T cells with or without the PARG inhibitor PDD00017273 (PARGin⁺ or PARGin⁻, respectively) in the lysis and IP buffer. Quantified in (F). Student's *t* tests. ***P* < 0.01; *****P* < 0.0001. Means ± SEM. (G) Phase diagram and (H and I) images of TAMRA-(GR)₂₀ (magenta) mixed with G3BP1-A488 (green) and PAR (2.5 to 25 μM MAR equivalents) or 25 μM MAR. Total molecules (1 μM) were fluorescently labeled. Buffer for condensation assays: PBS.

PAR promotes poly(GR)-induced TDP-43 aggregation

SG assembly can trigger TDP-43 aggregation (22). We and others have shown that poly(GR) promotes the aggregation of recombinant TDP-43, colocalizes with TDP-43 in SGs in cultured cells, and coaggregates with TDP-43 in postmortem tissue from patients with c9ALS/FTD (11, 14, 27). Together, these findings suggest that poly(GR) contributes to c9ALS/FTD pathogenesis by promoting TDP-43 aggregation.

To investigate whether PAR modulates poly(GR)-induced TDP-43 aggregation, we mixed TAMRA-(GR)₂₀ and A488-labeled recombinant TDP-43 (TDP-43-A488), with or without PAR. As shown in Fig. 6 (A and B), TAMRA-(GR)₂₀ and TDP-43-A488 formed irregularly shaped, aggregate-like condensates. Furthermore, PAR, but not MAR, promoted this process by inducing condensate formation at conditions in which the proteins do not form condensates without PAR. To quantify the amount of proteins in the condensates, we pel-

leted the condensates by centrifugation, dissolved them in urea buffer, and measured A488 and TAMRA fluorescent intensities (Fig. 6C). As shown in Fig. 6D, PAR, but not MAR, strongly increased the A488 signal in the pellet compared to the control, suggesting that PAR can promote poly(GR)-induced TDP-43 condensation. Of importance, little A488 signal was detected in the pellet if TAMRA-(GR)₂₀ was not included in the initial mixture (Fig. 6D), suggesting that PAR alone was unable to cause TDP-43 condensation in this condition.

or with PARGin removed from buffers. As shown in Fig. 5 (E and F), both methods reduced PAR and inhibited this interaction, suggesting that PAR enhances G3BP1 interaction with poly(GR). To test whether poly(GR) also promotes G3BP1 condensation, we mixed TAMRA-(GR)₂₀ with G3BP1-A488 and found that they formed condensates without a crowding agent (Fig. 5, G and H, and fig. S5D). Moreover, PAR promoted this process by inducing G3BP1/poly(GR) condensate formation at conditions in which the proteins do not form condensates without PAR (Fig. 5, G and I, and fig. S5, E and F). These data suggest that PAR promotes G3BP1 condensation and interaction with poly(GR).

To further test whether PAR promotes poly(GR)-induced TDP-43 condensation, we used a turbidity assay, which measures the increase

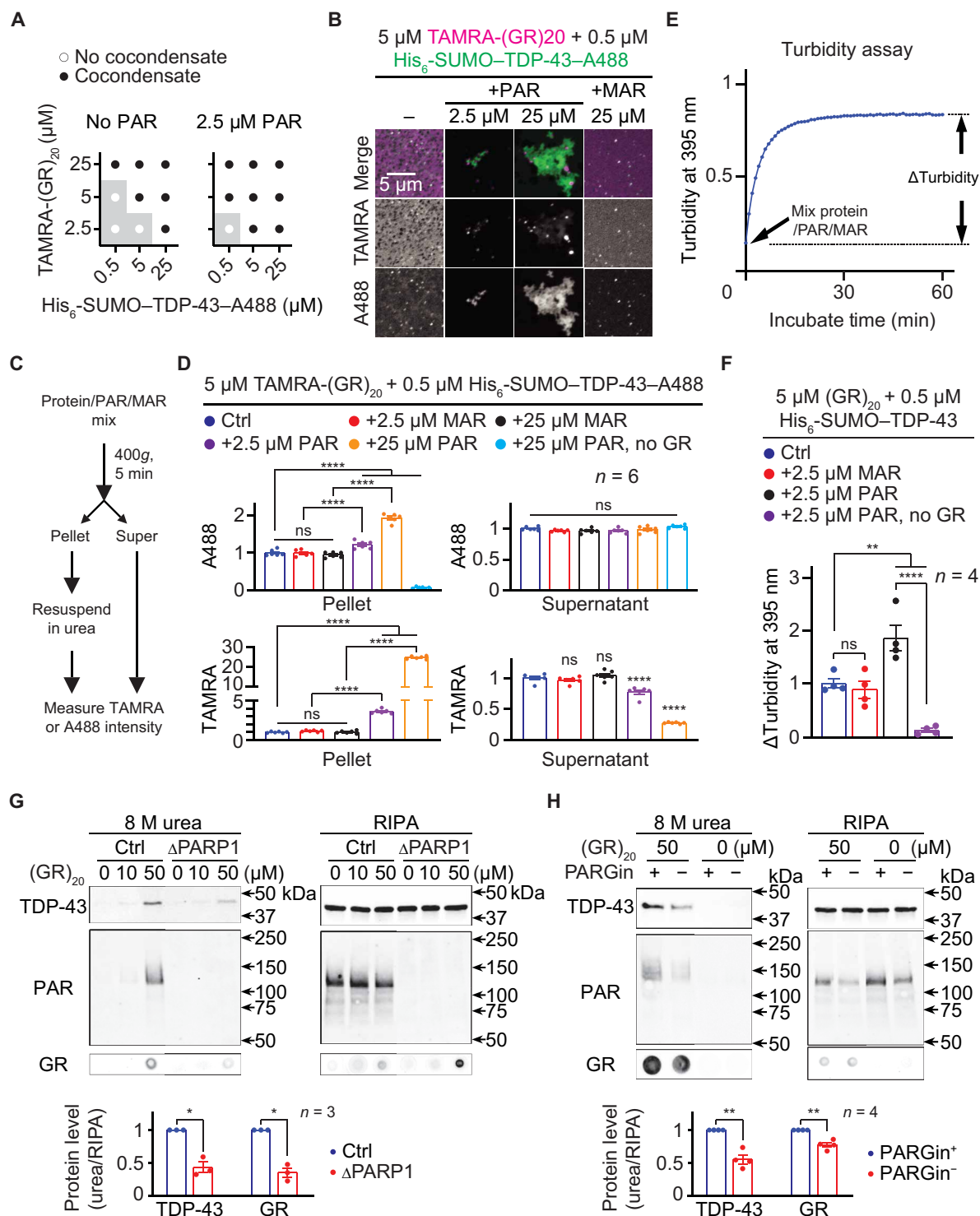


Fig. 6. PAR promotes poly(GR)-induced TDP-43 aggregation. (A) Phase diagram and (B) images of TAMRA-(GR)₂₀ (magenta) mixed with His₆-SUMO-TDP-43-A488 (green) and PAR (2.5 to 25 μM MAR equivalents) or 25 μM MAR. Total proteins were fluorescently labeled. Buffer: PBS. (C) The TDP-43 precipitation assay. (D) Quantification of A488 and TAMRA intensities. (E) The turbidity assay. (F) Quantification of increases in 395-nm absorbance. (G and H) Immunoblot of RIPA and urea fractions of control (Ctrl) or PARP1 KO (ΔPARP1) HEK293T cell lysate (G) or Ctrl HEK293T cell lysate with or without the PARG inhibitor PDD00017273 (PARGin⁺ or PARGin⁻, respectively; H), treated with (GR)₂₀. Quantification reported below. One-way ANOVA with Tukey's tests (D and F) and Student's *t* tests (G and H). **P* < 0.05, ***P* < 0.01, and *****P* < 0.0001. Means ± SEM.

in solution turbidity due to condensate formation (63). We mixed non-fluorescently labeled (GR)₂₀ and TDP-43 with or without PAR or MAR in solution and measured the increase in turbidity after a 60-min incubation (Fig. 6E). As shown in Fig. 6F, PAR, but not MAR, caused higher turbidity increase compared to controls. Also, little increase was observed if (GR)₂₀ was not included in the mix (Fig. 6F), consistent with our data in Fig. 6D. Together, these data strongly suggest that PAR promotes poly(GR)-induced TDP-43 condensation in vitro.

Next, we tested whether PAR promotes poly(GR)-induced TDP-43 aggregation in cultured cells. To induce endogenous TDP-43 aggregation, we used a previously published method in which chemically synthesized poly(GR) peptides were added to radioimmunoprecipitation assay (RIPA) buffer lysates of cells (64). As shown in Fig. 6 (G and H) and fig. S6, 50 μM (GR)₂₀, but not (GP)₂₀, caused endogenous TDP-43 and PAR, as well as (GR)₂₀ itself, to become RIPA insoluble but urea soluble. Furthermore, either PARP1 KO or removing PARGin from the cell lysis buffer reduced TDP-43 and (GR)₂₀ abundance in the urea versus RIPA fractions (Fig. 6, G and H), suggesting that PAR promotes poly(GR) and TDP-43 aggregation in cell lysates. In summary, our data suggest that PAR promotes poly(GR)-induced TDP-43 condensation and aggregation in vitro and in cell lysates, respectively.

Loss of PARP1/Parp suppresses R-DPR aggregation in C9ALS/FTD flies

To study whether PAR contributed to R-DPR aggregation in vivo, we performed dot blot on RIPA and urea extracts from aged fly heads expressing (GR)₃₆ or (PR)₃₆, with or without *parp* RNAi, under the control of GMR-GAL4. As shown in Fig. 7 (A and B) and S1B, *parp* RNAi reduced R-DPR in the urea versus RIPA fractions but not total R-DPR. Another fly model of c9ALS/FTD expresses 44 G₄C₂ repeats with a C-terminal GFP tag in the poly(GR) reading frame (65), which allows easy detection of poly(GR). We found that *parp* RNAi also suppressed eye degeneration (Fig. 7C) and poly(GR)-GFP in the urea versus RIPA fractions in this fly model (Fig. 7D), but not total GFP (fig. S1B). Together, our data suggest that *parp* loss suppresses R-DPR aggregation in fly models of c9ALS/FTD.

PAR associates with poly(GR) and TDP-43 aggregation in patient postmortem frontal cortices

To better probe the human relevance of our findings above, we investigated the relationships among insoluble PAR, poly(GR), and TDP-43 in postmortem frontal cortex tissue from 60 C9ORF72 repeat expansion carriers neuropathologically diagnosed with FTLN or FTLN with motor neuron disease (MND) (Fig. 7E and table S1).

We measured PAR and poly(GR) in RIPA-insoluble, urea-soluble frontal cortex fractions by dot blot followed by densitometry analyses. In addition, we used an established immunoassay (66) to measure TDP-43 with phosphoserines at 409 or 410 (pTDP-43), a pathologic form of TDP-43 (67, 68). As shown in Fig. 7F, insoluble PAR was positively associated with both poly(GR) and pTDP-43 in analyses adjusting for age, sex, and disease subtype (FTLN versus FTLN-MND), further supporting a relationship of PAR with poly(GR) and TDP-43 aggregation.

DISCUSSION

R-DPRs play a critical role in c9ALS/FTD pathogenesis. Both in vitro and in vivo evidence suggest that they exert their toxicity, at least in

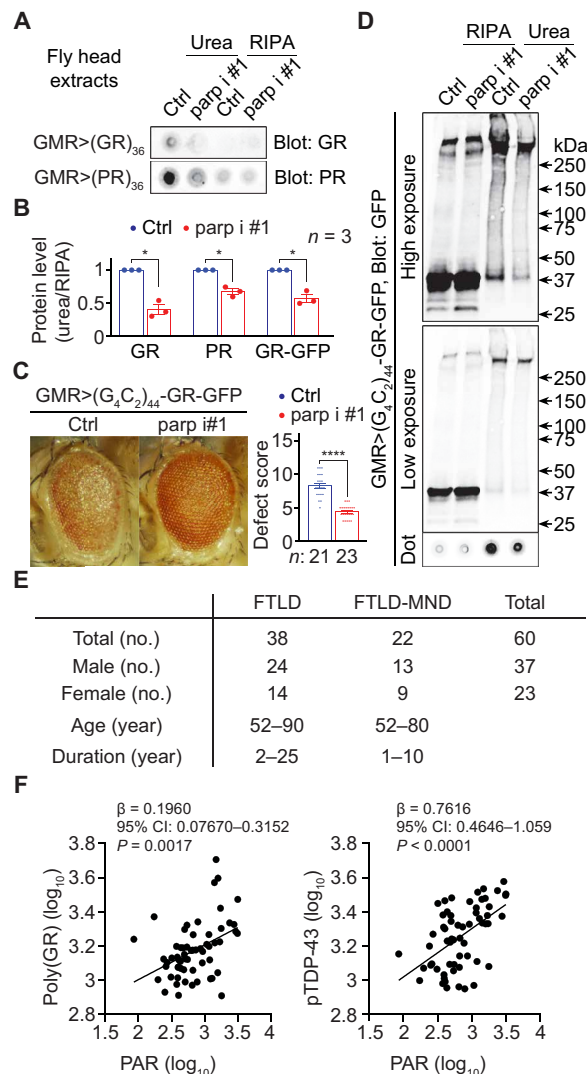


Fig. 7. PAR and protein aggregation in vivo. (A) Dot blots of RIPA and urea fractions of head extract from flies expressing R-DPRs without (Ctrl) or with coexpressing *parp* RNAi (*parp* i #1). (B) Quantification of (A) and (D). (C) Fly eyes expressing 44 G₄C₂ repeats with a C-terminal GFP tag in the poly(GR) reading frame [(G₄C₂)₄₄-GR-GFP] with or without coexpressing *parp* RNAi. (D) Immunoblot of RIPA and urea fractions of head extract from flies expressing (G₄C₂)₄₄-GR-GFP with or without coexpressing *parp* i #1. Student's *t* tests. **P* < 0.05 and *****P* < 0.0001. Means ± SEM. (E) c9ALS/FTD patient information. (F) Association of insoluble PAR with insoluble poly(GR) (left) or insoluble TDP-43 phosphorylated at S409/410 (pTDP-43) (right) in frontal cortex lysates from C9ORF72-repeat expansion carriers with frontotemporal lobar degeneration (FTLN) with or without motor neuron disease (MND). CI, confidence interval. Multiple linear regression.

part, by causing aberrant SG formation and inducing the aggregation of SG proteins such as TDP-43 (11, 13, 26, 27). However, how these processes are regulated is unclear. Here, we found that loss of PARP1 activity suppresses R-DPR-induced SG formation. Furthermore, PAR promotes R-DPR condensation and poly(GR) coaggregation with TDP-43, suggesting that it might contribute to R-DPR toxicity. Remaining questions include whether loss of PARylation suppresses R-DPR-induced SG formation and whether this can be rescued by restoring PAR or PARylation.

PARP1 acts as a first responder that detects DNA damage (28). Poly(GR) can cause DNA damage by increasing mitochondrial reactive oxygen species, whereas poly(GA) and G₄C₂ repeat RNAs can respectively disrupt the DNA repair machinery and generate R-loops, DNA/RNA complexes that can cause double-strand breaks (69, 70). Thus, further studies can test whether DNA damage causes increased PAR in c9ALS/FTD.

Protein aggregation is a common feature in neurodegenerative diseases. Previous studies showed that PAR promotes α -synuclein aggregation and toxicity in a Parkinson's disease model (48). Here, we show that PAR promotes R-DPR-induced TDP-43 aggregation and that PARP1 RNAi or PARP1 inhibitors suppress neurodegeneration in fly and iPSN models of c9ALS/FTD. When combined, these findings suggest an important role of PAR in promoting protein aggregation and neurodegeneration. It ought also be mentioned that, in addition to promoting protein aggregation, excessive PAR causes parthanatos and inhibits axonal growth (32, 71). In contrast, loss of PARP1 activity increases nicotinamide adenine dinucleotide (NAD), which can be beneficial to neurons (72). Hence, inhibiting PARP1 may suppress c9ALS/FTD neurodegenerative via multiple mechanisms.

Previous studies suggested that PAR can play either deleterious or beneficial roles in TDP-43 toxicity, depending on the research systems used. Knockdown of PARPs, PARG overexpression, or PARP1/2 inhibition suppresses neurodegeneration caused by TDP-43 overexpression in *Drosophila* or cultured neurons (30, 34, 47), suggesting that PAR contributes to TDP-43 toxicity. However, PAR also prevents pathological phase separation and aggregation and promotes the physiological LLPS of TDP-43 in vitro (46, 47), suggesting a beneficial role. We show here that PAR by itself does not trigger TDP-43 aggregation. Also, although poly(GP) causes PAR up-regulation, it does not result in cytotoxicity or TDP-43 aggregation. Conversely, PAR promotes poly(GR)-induced TDP-43 aggregation and contributes to poly(GR) toxicity. Hence, how PAR affects TDP-43 toxicity likely depends on additional TDP-43 regulators. TDP-43 aggregates in patient tissue contain other proteins (13, 27), and future studies can focus on how these proteins—PAR, poly(GR), and TDP-43—affect their coaggregation.

SG assembly is mediated by a network of inter and intramolecular interactions among SG proteins (18). Because many SG proteins are PARylated or bind to PAR (56, 61), PAR may foster SG assembly by providing additional valences to the network, thereby promoting condensation. Previous studies have shown that PAR induces LLPS of SG proteins TDP-43, and hnRNP A1 and PARP1 inhibitors respectively delay or suppress arsenite or DNA damage-induced SG assembly (29, 30). Consistent with this notion, we show that PAR induces G3BP1 condensation in vitro, and loss of PARP1 activity reduces R-DPR-induced SG assembly, suggesting a general role of PAR in protein condensation and SG formation. A remaining question is how PARP1, a mainly nuclear protein, causes PARylation of SG proteins in the cytoplasm. One possibility is that these proteins are PARylated in the nucleus before translocating the SGs; alternatively, they can be PARylated by cytoplasmic PARP1 or PARPs activated by PARP1.

SGs can trigger the aggregation of TDP-43 and other SG proteins and thus are believed to contribute to ALS/FTD pathogenesis. Although c9ALS/FTD iPSNs do not constitutively form SGs, they are constitutively under a certain degree of stress, as indicated by a mild increase in phospho-eIF2 α (14). Furthermore, loss of Ataxin-2

or SG inhibitors suppresses toxicity in yeast, animal, and iPSN models of c9- and TDP-43-ALS/FTD (14, 73–76). Here, we show that loss of PARP1 activity reduces SG formation and suppresses neurodegeneration in fly and cellular models of c9ALS/FTD, supporting a role of SG formation in pathogenesis. As several PARP1 inhibitors are Food and Drug Administration-approved or in advanced clinical trials for cancer treatment, and veliparib is neuroprotective in a mouse model of Parkinson's disease without detrimental side effects (48), these findings suggest potential clinical translations. As SGs were also implicated in neurodegeneration observed in mouse models of other diseases, including tauopathies, a prion disease, and a vanishing white matter disease (74, 77, 78), PAR likely also contributes to their pathogenesis. Hence, targeting PAR may be a therapeutic approach for these diseases.

To further test the potential of PAR as a therapeutic target for ALS and FTD, it is important to validate our findings in mammalian models in vivo. Several mouse models of c9- and TDP-43-ALS/FTD are available (13, 27, 73, 79), and future studies can test whether PARP1 KO or PARP inhibitors ameliorate neurodegeneration and behavioral defects in these models. Moreover, although nuclear PAR is up-regulated in brain neurons of patients with ALS/FTD (34), it is unclear about the amount of cytoplasmic PAR, which is more relevant to SG assembly and the aggregation of DPRs and TDP-43. In addition, it is unclear whether PAR in the cerebrospinal fluid is up-regulated in patients with c9ALS/FTD. Last, potential deleterious effects of PARP1 inhibition needs to be considered given the essential roles of PAR in cellular physiology. For instance, PARP1 inhibitors can suppress DNA damage repair and kill cells (28). In addition, PAR is essential to nucleolar structure and function (80). Thus, it is important to identify safe doses of PARP inhibitors when treating neurons.

MATERIALS AND METHODS

Study design

The goals of this study were to: (i) test the role of PARP1/PAR in fly and iPSN models of c9ALS/FTD, (ii) determine how PARP1/PAR affects R-DPR condensation in vitro and SG assembly in cultured cells, and (iii) investigate how PAR affects poly(GR) and TDP-43 aggregation in postmortem tissue of patients with c9ALS/FTD. As such, we performed fly eye degeneration and flight assays, toxicity assays in iPSNs, protein/PAR condensation assays, FRAP analyses, immunofluorescent staining, and Western blots. We also measured insoluble PAR, poly(GR), and pTDP-43 amounts in patient postmortem tissue.

Sample size for postmortem studies was determined on the basis of availability, whereas that for other studies was determined on the basis of previously published papers and current accepted standards according to journal policies. No statistical analysis was used to pre-determine sample size. All experiments were done with a minimum number of replicates based on previous expertise in statistical analyses of similar experimental datasets, and the statistical analysis demonstrates that our sample sizes revealed differences between groups. All data were unbiasedly collected, and no data were excluded from the study. The findings in this study were collected from multiple independent experiments and were reliably reproduced. The *n* numbers of each samples are indicated in the figure legend. Investigators were blinded to genotypes for the iPSN and cell culture experiments but not the fly experiments. Human tissues

were collected at Mayo Clinic with the approval of the Institutional Review Board. All patient information is Health Insurance Portability and Accountability Act compliant.

Drosophila

Flies were raised and maintained on yeast-cornmeal-syrup food at 25°C unless otherwise indicated (see below). Stocks and crosses were transferred to new vials on a regular basis. The UAS-PARG transgenic flies were made by Rainbow Transgenic Flies.

To assess eye defects, [*GMR-GAL4, UAS-(G₄C₂)₃₀/CyO, twi-GAL4, UAS-GFP*], [*GMR-GAL4, UAS-(GR)₃₆/CyO*], [*GMR-GAL4, UAS-(PR)₃₆/CyO*], or [*GMR-GAL4/CyO; UAS-LCS-(G₄C₂)₄₄-GR-GFP/MKRS*] flies were crossed to *Canton-S, UAS-parp RNAi*, or *UAS-PARG* flies, and nonbalancer, female flies were selected from the offspring and aged at 25°C for 15 days [for (*G₄C₂*)₃₀ or *44* flies] or not aged [for (*GR*)₃₆ and (*PR*)₃₆ flies]. Eye defects were quantified using a previously described method (36, 81). Briefly, points were added if there was a complete loss of interommatidial bristles, necrotic patches, retinal collapse, loss of ommatidial structure, and/or depigmentation of the eye. For drug feeding, dimethyl sulfoxide (DMSO) or 5 μM PJ34 was mixed in the fly food. Adult flies were transferred to new vials every 2 to 3 days.

For the flight assay, [*UAS-(G₄C₂)₃₀/CyO, elavGS-GAL4/MKRS*], [*UAS-(GR)₃₆/CyO, elavGS-GAL4/MKRS*], or [*UAS-(PR)₃₆/CyO, elavGS-GAL4/MKRS*] were crossed to *Canton-S, UAS-parp RNAi*, or *UAS-PARG* flies. Nonbalancer, female flies were selected and aged at 27°C for 12 days on regular food supplemented with 300 μM RU486 and either DMSO or 5 μM PJ34. Flies were transferred to fresh food every 2 to 3 days. After aging, individual flies were dropped into a graduated cylinder through a hole at the center of its lid. The cylinder was graduated into 12 zones of 25 mm each (top: 0; bottom: 12). The landing height was noted as the zone number in which the fly landed.

For protein extraction, fly heads were collected and homogenized in RIPA buffer supplemented with protease inhibitors. The homogenates were centrifuged at 1000g for 5 min, and the pellet was discarded. The supernatant was centrifuged at 18,000g for 20 min to separate the RIPA-soluble and insoluble fractions. The insoluble fraction was then washed with RIPA buffer with protease inhibitors and subsequently dissolved in the urea buffer [25 mM tris-HCl (pH 7.4), 150 mM NaCl, 2% SDS, and 8 M urea].

Human iPSCs

Isogenic pairs of iPSC lines were previously described (82). To confirm the presence or absence of the expanded *C9orf72* repeat in the c9-iso and Ctrl-iso iPSCs, respectively, we used the repeat-primed polymerase chain reaction (PCR) method previously described in (1). Briefly, genomic DNA (150 ng/μl) was PCR-amplified using a fluorescently labeled forward primer 5'-TGTAACACGACGGC-CAGTCAAGGAGGGAAACAACCGCAGCC-3', reverse primer 5'-CAGGAAACAGCTATGACCGGGCCCCGCCCGACCACGC-CCCCGGCCCCGGCCCCGG-3' and an M13R linker 5'-CAGGAAA-CA GCTATGACC-3', followed by fragment length analysis on an automated ABI3730 DNA analyzer and allele identification using GeneMapper v5.0 software (Applied Biosystems). The c9ALS/FTD sample with an expansion displays a characteristic stuttering pattern, whereas the isogenic controls does not (fig. S8).

Other iPSC lines were obtained from the Cedar Sinai Hospital iPSC core. All iPSCs were maintained in mTeSR media on Matrigel-coated

petri dishes. iPSCs are differentiated into motor neurons using the direct-induced motor neuron protocol (39). Briefly, growth factors were added at different stages to differentiate iPSCs to neuroepithelial cells, neural progenitor cells, and then motor neurons. Motor neurons were analyzed at days 32 to 36 of differentiation. Cells are maintained at 37°C in a humidified incubator supplemented with 5% CO₂. All cells are routinely tested negative for mycoplasma.

Glutamate toxicity assays were performed as previously described (39). Briefly, days 32 to 36 iPSCs pretreated with DMSO or PARP inhibitors for 2 days were challenged with 10 μM L-glutamate, together with DMSO or PARP inhibitors, for 4 hours in artificial cerebrospinal fluid. After that, cells were costained with PI (staining dead cells) and NucBlue (staining all cells) and live-imaged on a Zeiss 900 confocal microscope. The numbers of dead and total cells were counted.

For LDH assays, days 32 to 36 iPSCs pretreated with DMSO or PARP inhibitors for 2 days were treated with 5 μM chemically synthesized (DPR)₂₀, together with DMSO or PARP inhibitors, in iPSC culture media for another 2 days. LDH assays were performed using the CyQUANT LDH Cytotoxicity Assay Kit (Thermo Fisher Scientific) following the manufacturer's instructions.

Transformed human cells

HEK293T (of likely female origin due to lack of any trace of Y chromosome) and U-2 osteosarcoma (U-2 OS) cells (of female origin) were cultured in Dulbecco's modified Eagle's medium (Gibco) supplemented with 10% fetal bovine serum and 1% penicillin-streptomycin. All cells are maintained at 37°C in a humidified incubator supplemented with 5% CO₂. Transfection was performed using polyethylenimine (except for the experiments generating PARP1 KO cells). Cells were analyzed at indicated time points after transfection. For PARP inhibitor treatments, cells were pretreated for 2 hours before transfection. All cells are routinely tested negative for mycoplasma.

Co-IP and immunoblot

Forty-eight hours after transfection, cells were lysed in the lysis buffer [50 mM tris (pH 7.4), 150 mM NaCl, 1% Triton X-100, 1× Roche cOmplete protease inhibitor, and 10 μM PJ34, with or without 0.5 μM PDD00017273]. The lysate was centrifuged at 1500g for 20 min, and the supernatant was taken out and incubated with GFP-Trap beads (ChromoTek) at 4°C overnight. After that, the beads were precipitated by centrifugation at 1000g for 5 min and washed in lysis buffer three times at 4°C. The proteins were either eluted using Laemmli buffer for immunoblot or using 1% SDS for mass spectrometry analyses. For immunoblot on whole-cell lysates, cells were directly lysed in Laemmli buffer.

For immunoblot, proteins were separated on 4 to 15% SDS Mini-PROTEAN TGX Precast Gels (Bio-Rad) and transferred to nitrocellulose membranes. For dot blots, 2 μl of protein samples were dotted on nitrocellulose membranes and air-dried. Tris-buffered saline plus tween-20 (TBST) [50 mM tris (pH 7.4), 150 mM NaCl, and 0.1% Tween-20] with 5% milk was used for blocking, except for the GR and PR antibodies, for which this step was skipped. The following primary antibodies were used: rabbit anti-PAR (Millipore Sigma), rabbit anti-PARP1 (Abcam, ab32138), rabbit anti-GR (Proteintech), rabbit anti-PR (Proteintech), rabbit anti-G3BP1 (Abcam, ab181149), rabbit anti-Ataxin-2 (Bethyl), and rabbit anti-TDP-43 (Proteintech), 1:1000 as well as mouse anti-β-actin (Millipore) and hicken anti-GFP (Abcam, ab13970), 1:5000. All primary and

secondary antibodies were diluted in TBST with 5% milk, except for the GR and PR antibodies, which were diluted in TBST. Donkey anti-mouse, rabbit, or chicken antibodies were used at 1:1000 or 5000.

PAR synthesis

PAR was synthesized using either PARP1 or PARP5 as previously described (56, 83). Briefly, NAD⁺ was mixed with PARP1 or PARP5 and histones. After finishing the reaction, PAR was purified using liquid chromatography or phenol/chloroform extraction followed by alcohol precipitation.

Peptide synthesis and protein expression and purification

Twenty repeats of DPRs, both fluorescently labeled and unlabeled, were synthesized by Peptide 2.0 Inc. G3BP1 was bacterially expressed and purified as described previously (18) with modifications. Briefly, the glutathione S-transferase (GST)–G3BP1 fusion protein was expressed in BL21 (RIPL) bacteria and purified using a GSTrap HP column (Cytiva). The eluted fusion protein was treated with tobacco etch virus (TEV) protease (New England BioLabs) to remove the GST tag, and nontagged G3BP1 protein is further purified using an ENrich Q column followed by an ENrich SEC 70 column (Bio-Rad). Fast protein liquid chromatography (FPLC) was performed on an NGC Quest 10 Chromatography System (Bio-Rad). The protein concentration was determined by 280-nm absorbance, and the purity was confirmed on a 4 to 20% polyacrylamide gel.

His₆-SUMO N-terminally tagged TDP-43 was purified as described previously (47). Briefly, bacterially expressed proteins were purified using Ni-NTA agarose beads (QIAGEN) and subsequently buffer-exchanged to 50 mM Hepes (pH 7.5), 500 mM NaCl, 5% glycerol, and 5 mM dithiothreitol by dialysis. Purified proteins were flash-frozen in liquid N₂ and stored as aliquots at –80°C. Upon use, protein aliquots were thawed and centrifuged at 16,100g for 10 min at 4°C to remove preformed aggregates. Protein concentration was determined by Bradford assays (Bio-Rad), and the purity was confirmed on a 4 to 20% polyacrylamide gel.

Dot blot binding assay

R-DPR peptides or vehicle control, phosphate-buffered saline (PBS), was dotted on a nitrocellulose membrane that was subsequently let to dry. The membrane was then incubated in 1 μM PAR in TBST at 4°C overnight. The membrane was then washed in phosphate-buffered saline with tween-20 (PBST) and blotted for PAR, poly(GR), or poly(PR).

Fluorescent labeling of PAR and proteins

The terminal ADP-ribose of PAR was Cy5-labeled using a published method (56, 58). Briefly, PAR and Cy5–2′-deoxyadenosine 5′-triphosphate (Jena Bioscience) were mixed with poly[inosinic: polycytidylic acid (I:C)] and 2′-5′-oligoadenylate synthetase 1 in the labeling buffer. The mixture was incubated at 37°C for 2 hours, and PAR-Cy5 was subsequently high-performance liquid chromatography-purified. G3BP1 and TDP-43 were labeled using Alexa488 C5 Maleimide (Thermo Fisher Scientific) following the manufacturer's instructions.

In vitro phase separation and aggregation assays

Proteins and PAR were mixed at certain concentrations in PBS (pH 7.4) and dropped in a chamber formed by a glass slide, a coverslip, and a double-sided tape as a spacer. The chamber was set with the

glass slide on the top and the coverslip at the bottom and put at room temperature for 20 min before being imaged under a Zeiss 900 confocal microscope.

Foerster resonance energy transfer

Selected condensates were bleached by a 200 iteration of the Cy5 laser (excitation: 640 nm) and then imaged every second. The intensity of the condensates was quantified by software affiliated to the Zeiss 900 confocal microscope.

Molecular cloning

To generate the pUAS-attB-PARG construct, the human PARG cDNA (OriGene) was PCR-amplified and cloned into the pUAS-attB vector (84) using Eco RI and Xho I restriction enzyme sites. To generate mCherry-(R-DPR)₅₀ constructs, the GFP coding sequences in the pEGFP-(R-DPR)₅₀ constructs (45) were replaced with mCherry coding sequences using Bam HI and Xba I restriction enzyme sites.

Fluorescent recovery after photobleaching

Condensates with similar sizes were randomly selected and bleached by laser at room temperature. After that, pictures were taken every second. The recovery percentage was calculated as $(I_{rec} - I_0) / (I_{pre} - I_0)$, in which I_{rec} , I_0 , and I_{pre} are the fluorescent intensity of the analyzed condensate after recovery, immediately after bleaching, and before bleaching, respectively. The diameters of selected condensates are ~2 for TAMRA-(GR)₂₀ and G3BP1 and ~1.5 for TAMRA-(PR)₂₀.

Turbidity assay

(GR)₂₀, TDP-43, PAR, or MAR were mixed at indicated concentration in PBS (pH 7.4) in 96-well plates. The absorbance of the solution mix at 395 nm was monitored for 60 min using a Tecan Spark Multimode Microplate Reader.

Generating PARP1 KO HEK293T cells

The PARP1 KO HEK293T cell line was generated using a previously described method (48) with modifications. Briefly, HEK293T cells were transfected with the pLentiCRISPR V2-PARP1–single-guide RNA (sgRNA) plasmids using the Effectene Transfection Reagent (QIAGEN) according to the manufacturer's instruction. In a parallel set of experiments to generate the control HEK293T cell line, the pLentiCRISPR V2 empty vector was used in transfection. Two days after transfection, cells were treated with puromycin (2 μg/μl; Sigma-Aldrich) and maintained in the same media for up to 2 weeks. Single cells were sorted using a fluorescence-activated cell sorting Aria cell sorter (BD bioscience) and plated, and individual single cell-originated clones were propagated and checked for PARP1 KO. The following sgRNAs were used to target *PARP1* Exon I (29 base pairs from the starting ATG site): PARP1-sgRNA#1 (5′-CACCG-GAGTCGAGTACGCCAAGAGC-3′) and PARP1-sgRNA#2 (5′-AAACGCTCTTGGCGTACTCGACTCC-3′).

TDP-43 aggregation in HEK293T cell lysates

Wild-type or PARP1 KO HEK293T cells were lysed in RIPA buffer [25 mM Tris-HCl (pH 7.4), 150 mM NaCl, 0.5% sodium deoxycholate, 1% NP-40, and 0.1% SDS] supplemented with protease inhibitors (Roche) and 10 μM PJ34, with or without 0.5 μM PDD00017273. Lysates were centrifuged at 1500g for 5 min, and the pellet was removed. (GR)₂₀ peptides were added to the supernatant, which is

then centrifuged at 18,000g for 10 min to separate the RIPA buffer-soluble and insoluble fractions. The insoluble fraction was washed in the same buffer used for cell lysis and dissolved in the urea buffer [50 mM tris (pH 7.4), 2% SDS, and 8 M urea].

Immunofluorescence staining

Cultured cells were fixed in 4% paraformaldehyde for 20 min and then penetrated in PBS with 0.1% Triton X-100 for 10 min. After that, cells were incubated in PBST buffer (PBS with 0.1% Tween 20) with 3% donkey serum and primary antibodies for 16 hours at 4°C. Primary antibodies were used at 1:100 dilution. Next, cells were washed in PBST at room temperature. Donkey secondary antibodies conjugated to Alexa Fluor 568 or 488 (Thermo Fisher Scientific) were used at 1:1000 dilution in PBST with 3% donkey serum. After incubating with secondary antibodies, cells were washed in PBST, mounted in ProLong Antifade Gold with 4',6-diamidino-2-phenylindole (DAPI), and subjected to confocal microscopy analyses.

Confocal microscopy

Confocal images were acquired using an LSM900 confocal microscope (Carl Zeiss) with accompanying software and Plan Apochromat 63×, numerical aperture 1.4 objectives (Carl Zeiss) at 37°C (for live-cell imaging) or room temperature (for all other types of imaging). Images were captured by an AxioCam HRc camera (Carl Zeiss) and were processed using ImageJ/Fiji (National Institutes of Health).

Preparing urea-soluble lysates from human frontal cortex tissues

Urea-soluble lysates from frontal cortex tissues were prepared as previously described (85). Tissue was homogenized in prechilled RIPA buffer supplemented with protease and phosphatase inhibitors and sonicated on ice. Homogenates were cleared by centrifugation at 100,000g for 30 min at 4°C. The supernatant was saved, and, to prevent carry-over, the resulting pellet was resuspended in RIPA buffer, resonicated, and recentrifuged. To the final insoluble pellet, 7 M urea buffer was added, followed by sonication, vortexing for 30 min, and centrifugation at 100,000g for 30 min at 22°C. The protein concentration of the urea-soluble supernatant was determined by Bradford assays.

pTDP-43 MSD immunoassay

The abundance of pTDP-43 in frontal cortex urea-soluble fractions was evaluated using a sandwich immunoassay that uses Meso Scale Discovery (MSD) electrochemiluminescence detection technology (66). A mouse monoclonal antibody that detects TDP-43 phosphorylated at serines 409 and 410 (1:500; #CAC-TIP-PTD-M01, Cosmo Bio, USA) was used as the capture antibody. The detection antibody was a rabbit polyclonal C-terminal TDP-43 antibody (2 µg/ml; 12892-1-AP, Proteintech) paired with a Sulfo tag-labeled goat anti-rabbit secondary antibody (1 µg/ml; R32AB-1, Meso Scale Diagnostics). Fractions were diluted in tris-buffered saline, and 35 µg of protein per well was assayed in duplicate wells. Response values (arbitrary units) corresponding to the intensity of emitted light upon electrochemical stimulation of the assay plate using the MSD QuickPlex SQ120 were acquired.

PAR, poly(GR), and pTDP-43 association analyses

Frontal cortex insoluble PAR, poly(GR), and pTDP-43 were normalized against total protein concentrations in the urea fraction and

log-transformed. Associations among the transformed values were examined using multiple linear regression models adjusted for age, sex, and disease subtype (FTLD versus FTLD with MND). β coefficients and 95% confidence intervals were estimated. *P* values of <0.025 were considered as significant after using a Bonferroni adjustment for multiple testing.

Statistical analysis

To quantify fluorescent or Western blot intensities, certain areas/bands were circled, and the intensities were measured using ImageJ/Fiji. Statistical analyses were performed using the GraphPad Prism 9.0 software. Tests used and levels of significance for each experiment are explained in each figure legend.

SUPPLEMENTARY MATERIALS

www.science.org/doi/10.1126/scitranslmed.abq3215

Figs. S1 to S7

Tables S1 and S2

Data file S1

[View/request a protocol for this paper from Bio-protocol.](#)

REFERENCES AND NOTES

1. M. DeJesus-Hernandez, I. R. Mackenzie, B. F. Boeve, A. L. Boxer, M. Baker, N. J. Rutherford, A. M. Nicholson, N. C. A. Finch, H. Flynn, J. Adamson, N. Kouri, A. Wojtas, P. Sengdy, G.-Y. R. Hsiung, A. Karydas, W. W. Seeley, K. A. Josephs, G. Coppola, D. H. Geschwind, Z. K. Wszolek, H. Feldman, D. S. Knopman, R. C. Petersen, B. L. Miller, D. W. Dickson, K. B. Boylan, N. R. Graff-Radford, R. Rademakers, Rademakers R. Expanded GGGGCC hexanucleotide repeat in noncoding region of C9ORF72 causes chromosome 9p-linked FTD and ALS. *Neuron* **72**, 245–256 (2011).
2. A. E. Renton, E. Majounie, A. Waite, J. Simón-Sánchez, S. Rollinson, J. R. Gibbs, J. C. Schymick, H. Laaksovirta, J. van Swieten, L. Myllykangas, H. Kalimo, A. Paetau, Y. Abramzon, A. M. Remes, A. Kaganovich, S. W. Scholz, J. Duckworth, J. Ding, D. W. Harmer, D. G. Hernandez, J. O. Johnson, K. Mok, M. Ryten, D. Trabzuni, R. J. Guerreiro, R. W. Orrell, J. Neal, A. Murray, J. Pearson, I. E. Jansen, D. Sondervan, H. Seelaar, D. Blake, K. Young, N. Halliwell, J. B. Callister, G. Toulson, A. Richardson, A. Gerhard, J. Snowden, D. Mann, D. Neary, M. A. Nalls, T. Peuralinna, L. Jansson, V. M. Isoviita, A. L. Kaivorinne, M. Hölttä-Vuori, E. Ikonen, R. Sulkava, M. Benatar, J. Wu, A. Chiò, G. Restagno, G. Borghero, M. Sabatelli; ITALSGEN Consortium, D. Heckerman, E. Rogava, L. Zinman, J. D. Rothstein, M. Sendtner, C. Drepper, E. E. Eichler, C. Alkan, Z. Abdullaev, S. D. Pack, A. Dutra, E. Pak, J. Hardy, A. Singleton, N. M. Williams, P. Heutink, S. Pickering-Brown, H. R. Morris, P. J. Tienari, B. J. Traynor, A hexanucleotide repeat expansion in C9ORF72 is the cause of chromosome 9p21-linked ALS-FTD. *Neuron* **72**, 257–268 (2011).
3. K. Mori, T. Arzberger, F. A. Grässer, I. Gijselink, S. May, K. Rentzsch, S. M. Weng, M. H. Schludi, J. van der Zee, M. Cruts, C. van Broeckhoven, E. Kremmer, H. A. Kretschmar, C. Haass, D. Edbauer, Bidirectional transcripts of the expanded C9orf72 hexanucleotide repeat are translated into aggregating dipeptide repeat proteins. *Acta Neuropathol.* **126**, 881–893 (2013).
4. K. Mori, S. M. Weng, T. Arzberger, S. May, K. Rentzsch, E. Kremmer, B. Schmid, H. A. Kretschmar, M. Cruts, C. van Broeckhoven, C. Haass, D. Edbauer, The C9orf72 GGGGCC repeat is translated into aggregating dipeptide-repeat proteins in FTLD/ALS. *Science* **339**, 1335–1338 (2013).
5. T. Zu, Y. Liu, M. Bañez-Coronel, T. Reid, O. Pletnikova, J. Lewis, T. M. Miller, M. B. Harms, A. E. Falchook, S. H. Subramony, L. W. Ostrow, J. D. Rothstein, J. C. Troncoso, L. P. W. Ranum, RAN proteins and RNA foci from antisense transcripts in C9ORF72 ALS and frontotemporal dementia. *Proc. Natl. Acad. Sci. U.S.A.* **110**, E4968–E4977 (2013).
6. P. E. A. Ash, K. F. Bieniek, T. F. Gendron, T. Caulfield, W.-L. Lin, M. DeJesus-Hernandez, M. M. van Blitterswijk, K. Jansen-West, J. W. Paul III, R. Rademakers, K. B. Boylan, D. W. Dickson, L. Petrucelli, Unconventional translation of C9ORF72 GGGGCC expansion generates insoluble polypeptides specific to c9FTD/ALS. *Neuron* **77**, 639–646 (2013).
7. C. J. Donnelly, P. W. Zhang, J. T. Pham, A. R. Hauesler, N. A. Mistry, S. Vidsensky, E. L. Daley, E. M. Poth, B. Hoover, D. M. Fines, N. Maragakis, P. J. Tienari, L. Petrucelli, B. J. Traynor, J. Wang, F. Rigo, C. F. Bennett, S. Blackshaw, R. Sattler, J. D. Rothstein, RNA toxicity from the ALS/FTD C9ORF72 expansion is mitigated by antisense intervention. *Neuron* **80**, 415–428 (2013).
8. T. F. Gendron, K. F. Bieniek, Y. J. Zhang, K. Jansen-West, P. E. A. Ash, T. Caulfield, L. Daugherty, J. H. Dunmore, M. Castanedes-Casey, J. Chew, D. M. Cosio, M. van Blitterswijk, W. C. Lee, R. Rademakers, K. B. Boylan, D. W. Dickson, L. Petrucelli, Antisense transcripts

- of the expanded C9orf72 hexanucleotide repeat form nuclear RNA foci and undergo repeat-associated non-ATG translation in c9FTD/ALS. *Acta Neuropathol.* **126**, 829–844 (2013).
9. S. Mzielinska, S. Grönke, T. Niccoli, C. E. Ridler, E. L. Clayton, A. Devoy, T. Moens, F. E. Norona, I. O. C. Woollacott, J. Pietrzyk, K. Cleverley, A. J. Nicoll, S. Pickering-Brown, J. Dols, M. Cabecinha, O. Hendrich, P. Fratta, E. M. C. Fisher, L. Partridge, A. M. Isaacs, C9orf72 repeat expansions cause neurodegeneration in *Drosophila* through arginine-rich proteins. *Science* **345**, 1192–1194 (2014).
 10. I. Kwon, S. Xiang, M. Kato, L. Wu, P. Theodoropoulos, T. Wang, J. Kim, J. Yun, Y. Xie, S. L. McKnight, Poly-dipeptides encoded by the C9orf72 repeats bind nucleoli, impede RNA biogenesis, and kill cells. *Science* **345**, 1139–1145 (2014).
 11. K. H. Lee, P. Zhang, H. J. Kim, D. M. Mitrea, M. Sarkar, B. D. Freibaum, J. Cika, M. Coughlin, J. Messing, A. Molliex, B. A. Maxwell, N. C. Kim, J. Temirov, J. Moore, R. M. Kolaitis, T. I. Shaw, B. Bai, J. Peng, R. W. Kriwacki, J. P. Taylor, C9orf72 dipeptide repeats impair the assembly, dynamics, and function of membrane-less organelles. *Cell* **167**, 774–788.e17 (2016).
 12. Y. Lin, E. Mori, M. Kato, S. Xiang, L. Wu, I. Kwon, S. L. McKnight, Toxic PR poly-dipeptides encoded by the C9orf72 repeat expansion target LC domain polymers. *Cell* **167**, 789–802.e12 (2016).
 13. Y.-L. Zhang, T. F. Gendron, M. T. W. Ebbert, A. D. O'Raw, M. Yue, K. Jansen-West, X. Zhang, M. Prudencio, J. Chew, C. N. Cook, L. M. Daugherty, J. Tong, Y. Song, S. R. Pickles, M. Castanedes-Casey, A. Kurti, R. Rademakers, B. Oskarsson, D. W. Dickson, W. Hu, A. D. Gitler, J. D. Fryer, L. Petrucelli, Poly(GR) impairs protein translation and stress granule dynamics in C9orf72-associated frontotemporal dementia and amyotrophic lateral sclerosis. *Nat. Med.* **24**, 1136–1142 (2018).
 14. K. Zhang, J. G. Daigle, K. M. Cunningham, A. N. Coyne, K. Ruan, J. C. Grima, K. E. Bowen, H. Wadhwa, P. Yang, F. Rigo, J. P. Taylor, A. D. Gitler, J. D. Rothstein, T. E. Lloyd, Stress granule assembly disrupts nucleocytoplasmic transport. *Cell* **173**, 958–971.e17 (2018).
 15. Y. J. Zhang, L. Guo, P. K. Gonzales, T. F. Gendron, Y. Wu, K. Jansen-West, A. D. O'Raw, S. R. Pickles, M. Prudencio, Y. Carlomagno, M. A. Gachechiladze, C. Ludwig, R. Tian, J. Chew, M. DeTure, W. L. Lin, J. Tong, L. M. Daugherty, M. Yue, Y. Song, J. W. Andersen, M. Castanedes-Casey, A. Kurti, A. Datta, G. Antognetti, A. McCampbell, R. Rademakers, B. Oskarsson, D. W. Dickson, M. Kampmann, M. E. Ward, J. D. Fryer, C. D. Link, J. Shorter, L. Petrucelli, Heterochromatin anomalies and double-stranded RNA accumulation underlie C9orf72 poly(PR) toxicity. *Science* **363**, eaav2606 (2019).
 16. N. Sakae, K. F. Bieniek, Y. J. Zhang, K. Ross, T. F. Gendron, M. E. Murray, R. Rademakers, L. Petrucelli, D. W. Dickson, Poly-GR dipeptide repeat polymers correlate with neurodegeneration and clinicopathological subtypes in C9orf72-related brain disease. *Acta Neuropathol. Commun.* **6**, 63 (2018).
 17. D. S. W. Protter, R. Parker, Principles and properties of stress granules. *Trends Cell Biol.* **26**, 668–679 (2016).
 18. P. Yang, C. Mathieu, R.-M. Kolaitis, P. Zhang, J. Messing, U. Yurtsever, Z. Yang, J. Wu, Y. Li, Q. Pan, J. Yu, E. W. Martin, T. Mittag, H. J. Kim, J. P. Taylor, G3BP1 is a tunable switch that triggers phase separation to assemble stress granules. *Cell* **181**, 325–345.e28 (2020).
 19. D. W. Sanders, N. Kedersha, D. S. W. Lee, A. R. Strom, V. Drake, J. A. Riback, D. Bracha, J. M. Eeftens, A. Iwanicki, A. Wang, M.-T. Wei, G. Whitney, S. M. Lyons, P. Anderson, W. M. Jacobs, P. Ivanov, C. P. Brangwynne, Competing protein-RNA interaction networks control multiphase intracellular organization. *Cell* **181**, 306–324.e28 (2020).
 20. J. Guillen-Boixet, A. Kopach, A. S. Holehouse, S. Wittmann, M. Jahnel, R. Schlüßler, K. Kim, I. R. E. A. Trussina, J. Wang, D. Mateju, I. Poser, S. Maharana, M. Ruer-Gruß, D. Richter, X. Zhang, Y.-T. Chang, J. Guck, A. Honigsmann, J. Mahamid, A. A. Hyman, R. V. Pappu, S. Alberti, T. M. Franzmann, RNA-induced conformational switching and clustering of G3BP drive stress granule assembly by condensation. *Cell* **181**, 346–361.e17 (2020).
 21. Y. Lin, D. S. W. Protter, M. K. Rosen, R. Parker, Formation and maturation of phase-separated liquid droplets by RNA-binding proteins. *Mol. Cell* **60**, 208–219 (2015).
 22. Y. R. Li, O. D. King, J. Shorter, A. D. Gitler, Stress granules as crucibles of ALS pathogenesis. *J. Cell Biol.* **201**, 361–372 (2013).
 23. N. Fernandes, L. Nero, S. Lyons, P. Ivanov, T. Mittelmeier, T. Bolger, J. Buchan, Stress granule assembly can facilitate but is not required for TDP-43 cytoplasmic aggregation. *Biomolecules* **10**, 1367 (2020).
 24. M. Hofweber, S. Hutten, B. Bourgeois, E. Spreitzer, A. Niedner-Boblentz, M. Schifferer, M.-D. Ruepp, M. Simons, D. Niessing, T. Madl, D. Dormann, Phase separation of FUS is suppressed by its nuclear import receptor and arginine methylation. *Cell* **173**, 706–719.e13 (2018).
 25. H. J. Kim, N. C. Kim, Y.-D. Wang, E. A. Scarborough, J. Moore, Z. Diaz, K. S. MacLea, B. Freibaum, S. Li, A. Molliex, A. P. Kanagaraj, R. Carter, K. B. Boylan, A. M. Wojtas, R. Rademakers, J. L. Pinkus, S. A. Greenberg, J. Q. Trojanowski, B. J. Traynor, B. N. Smith, S. Topp, A.-S. Gkazi, J. Miller, C. E. Shaw, M. Kottlors, J. Kirschner, A. Pestronk, Y. R. Li, A. F. Ford, A. D. Gitler, M. Benatar, O. D. King, V. E. Kimonis, E. D. Ross, C. C. Weihl, J. Shorter, J. P. Taylor, Mutations in prion-like domains in hnRNPA2B1 and hnRNPA1 cause multisystem proteinopathy and ALS. *Nature* **495**, 467–473 (2013).
 26. S. Boeynaems, E. Bogaert, D. Kovacs, A. Konijnenberg, E. Timmerman, A. Volkov, M. Guharoy, M. de Decker, T. Jaspers, V. H. Ryan, A. M. Janke, P. Baatsen, T. Vercurryse, R.-M. Kolaitis, D. Daelemans, J. P. Taylor, N. Kedersha, P. Anderson, F. Impens, F. Sobott, J. Schymkowitz, F. Rousseau, N. L. Fawzi, W. Robberecht, P. van Damme, P. Tompa, L. van den Bosch, Phase separation of C9orf72 dipeptide repeats perturbs stress granule dynamics. *Mol. Cell* **65**, 1044–1055.e5 (2017).
 27. C. N. Cook, Y. Wu, H. M. Odeh, T. F. Gendron, K. Jansen-West, G. del Rosso, M. Yue, P. Jiang, E. Gomes, J. Tong, L. M. Daugherty, N. M. Avendano, M. Castanedes-Casey, W. Shao, B. Oskarsson, G. S. Tomassy, A. McCampbell, F. Rigo, D. W. Dickson, J. Shorter, Y.-J. Zhang, L. Petrucelli, C9orf72 poly(GR) aggregation induces TDP-43 proteinopathy. *Sci. Transl. Med.* **12**, eabb3774 (2020).
 28. A. Ray Chaudhuri, A. Nussenzweig, The multifaceted roles of PARP1 in DNA repair and chromatin remodelling. *Nat. Rev. Mol. Cell Biol.* **18**, 610–621 (2017).
 29. M. Isabelle, J. P. Gagné, I. E. Gallouzi, G. G. Poirier, Quantitative proteomics and dynamic imaging reveal that G3BP-mediated stress granule assembly is poly(ADP-ribose)-dependent following exposure to MNNG-induced DNA alkylation. *J. Cell Sci.* **125**(Pt 19), 4555–4566 (2012).
 30. Y. Duan, A. du, J. Gu, G. Duan, C. Wang, X. Gui, Z. Ma, B. Qian, X. Deng, K. Zhang, L. Sun, K. Tian, Y. Zhang, H. Jiang, C. Liu, Y. Fang, PARylation regulates stress granule dynamics, phase separation, and neurotoxicity of disease-related RNA-binding proteins. *Cell Res.* **29**, 233–247 (2019).
 31. S. Hanai, M. Kanai, S. Ohashi, K. Okamoto, M. Yamada, H. Takahashi, M. Miwa, Loss of poly(ADP-ribose) glycohydrolase causes progressive neurodegeneration in *Drosophila melanogaster*. *Proc. Natl. Acad. Sci. U.S.A.* **101**, 82–86 (2004).
 32. S. A. Andrabi, N. S. Kim, S. W. Yu, H. Wang, D. W. Koh, M. Sasaki, J. A. Klaus, T. Otsuka, Z. Zhang, R. C. Koehler, P. D. Hurn, G. G. Poirier, V. L. Dawson, T. M. Dawson, Poly(ADP-ribose) (PAR) polymer is a death signal. *Proc. Natl. Acad. Sci. U.S.A.* **103**, 18308–18313 (2006).
 33. D. W. Koh, A. M. Lawler, M. F. Poiras, M. Sasaki, S. Wattler, M. C. Nehls, T. Stöger, G. G. Poirier, V. L. Dawson, T. M. Dawson, Failure to degrade poly(ADP-ribose) causes increased sensitivity to cytotoxicity and early embryonic lethality. *Proc. Natl. Acad. Sci. U.S.A.* **101**, 17699–17704 (2004).
 34. L. McGurk, J. Mojsilovic-Petrovic, V. M. van Deerlin, J. Shorter, R. G. Kalb, V. M. Lee, J. Q. Trojanowski, E. B. Lee, N. M. Bonini, Nuclear poly(ADP-ribose) activity is a therapeutic target in amyotrophic lateral sclerosis. *Acta Neuropathol. Commun.* **6**, 84 (2018).
 35. A. H. Brand, N. Perrimon, Targeted gene expression as a means of altering cell fates and generating dominant phenotypes. *Development* **118**, 401–415 (1993).
 36. K. Zhang, C. J. Donnelly, A. R. Haeusler, J. C. Grima, J. B. Machamer, P. Steinwald, E. L. Daley, S. J. Miller, K. M. Cunningham, S. Vidsensky, S. Gupta, M. A. Thomas, I. Hong, S. L. Chiu, R. L. Huganir, L. W. Ostrow, M. J. Matunis, J. Wang, R. Sattler, T. E. Lloyd, J. D. Rothstein, The C9orf72 repeat expansion disrupts nucleocytoplasmic transport. *Nature* **525**, 56–61 (2015).
 37. L. D. Goodman, M. Prudencio, N. J. Kramer, L. F. Martinez-Ramirez, A. R. Srinivasan, M. Lan, M. J. Parisi, Y. Zhu, J. Chew, C. N. Cook, A. Berson, A. D. Gitler, L. Petrucelli, N. M. Bonini, Toxic expanded GGGGCC repeat transcription is mediated by the PAF1 complex in C9orf72-associated FTD. *Nat. Neurosci.* **22**, 863–874 (2019).
 38. M. Murawska, M. Hassler, R. Renkawitz-Pohl, A. Ladurner, A. Brehm, Stress-induced PARP activation mediates recruitment of *Drosophila* Mi-2 to promote heat shock gene expression. *PLoS Genet.* **7**, e1002206 (2011).
 39. A. N. Coyne, B. L. Zaepfel, L. Hayes, B. Fitchman, Y. Salzberg, E.-C. Luo, K. Bowen, H. Trost, S. Aigner, F. Rigo, G. W. Yeo, A. Harel, C. N. Svendsen, D. Sareen, J. D. Rothstein, G4C2 repeat RNA initiates a POM121-mediated reduction in specific nucleoporins in C9orf72 ALS/FTD. *Neuron* **107**, 1124–1140.e11 (2020).
 40. E. G. Baxi, T. Thompson, J. Li, J. A. Kaye, R. G. Lim, J. Wu, D. Ramamoorthy, L. Lima, V. Vaibhav, A. Matlock, A. Frank, A. N. Coyne, B. Landin, L. Ornelas, E. Mosmiller, S. Thrower, S. M. Farr, L. Panther, E. Gomez, E. Galvez, D. Perez, I. Meepe, S. Lei, B. Mandefro, H. Trost, L. Pinedo, M. G. Banuelos, C. Liu, R. Moran, V. Garcia, M. Workman, R. Ho, S. Wyman, J. Roggenbuck, M. B. Harms, J. Stocksdale, R. Miramontes, K. Wang, V. Venkatraman, R. Holewinski, N. Sundararaman, R. Pandey, D.-M. Manalo, A. Donde, N. Huynh, M. Adam, B. T. Wassie, E. Vertudes, N. Amirani, K. Raja, R. Thomas, L. Hayes, A. Lenail, A. Cerezo, S. Luppino, A. Farrar, L. Pothier, C. Prina, T. Morgan, A. Jamil, S. Heintzman, J. Jockel-Balsarotti, E. Karanja, J. Markway, M. McCallum, B. Joslin, D. Alibazoglu, S. Kolb, S. Ajroud-Driss, R. Baloh, D. Heitzman, T. Miller, J. D. Glass, N. L. Patel-Murray, H. Yu, E. Sinani, P. Vigneswaran, A. V. Sherman, O. Ahmad, P. Roy, J. C. Beavers, S. Zeiler, J. W. Krakauer, C. Arguto, G. Cecchi, M. Bellard, Y. Raghav, K. Sachs, T. Ehrenberger, E. Bruce, M. E. Cudkowicz, N. Maragakis, R. Norel, J. E. van Eyk, S. Finkbeiner, J. Berry, D. Sareen, L. M. Thompson, E. Fraenkel, C. N. Svendsen, J. D. Rothstein, Answer ALS, a large-scale resource for sporadic and familial ALS combining clinical and multi-omics data from induced pluripotent cell lines. *Nat. Neurosci.* **25**, 226–237 (2022).
 41. A. N. Coyne, V. Baskerville, B. L. Zaepfel, D. W. Dickson, F. Rigo, F. Bennett, C. P. Lusk, J. D. Rothstein, Nuclear accumulation of CHMP7 initiates nuclear pore complex injury

- and subsequent TDP-43 dysfunction in sporadic and familial ALS. *Sci. Transl. Med.* **13**, ea1923 (2021).
42. Y. Shi, S. Lin, K. A. Staats, Y. Li, W.-H. Chang, S.-T. Hung, E. Hendricks, G. R. Linares, Y. Wang, E. Y. Son, X. Wen, K. Kislser, B. Wilkinson, L. Menendez, T. Sugawara, P. Woolwine, M. Huang, M. J. Cowan, B. Ge, N. Koutsodendris, K. P. Sandor, J. Komberg, V. R. Vangoor, K. Senthilkumar, V. Hennes, C. Seah, A. R. Nelson, T.-Y. Cheng, S.-J. Lee, P. R. August, J. A. Chen, N. Wisniewski, V. Hanson-Smith, T. G. Belgard, A. Zhang, M. Caba, C. Grunseich, M. E. Ward, L. H. van den Berg, R. J. Pasterkamp, D. Trotti, B. V. Zlokovic, J. K. Ichida, Haploinsufficiency leads to neurodegeneration in C9ORF72 ALS/FTD human induced motor neurons. *Nat. Med.* **24**, 313–325 (2018).
 43. J. D. Rothstein, L. J. Martin, R. W. Kuncl, Decreased glutamate transport by the brain and spinal cord in amyotrophic lateral sclerosis. *N. Engl. J. Med.* **326**, 1464–1468 (1992).
 44. Y. J. Zhang, T. F. Gendron, J. C. Grima, H. Sasaguri, K. Jansen-West, Y.-F. Xu, R. B. Katzman, J. Gass, M. E. Murray, M. Shinohara, W.-L. Lin, A. Garrett, J. N. Stankowski, L. Daugherty, J. Tong, E. A. Perkerson, M. Yue, J. Chew, M. Castanedes-Casey, A. Kurtz, Z. S. Wang, A. M. Liesinger, J. D. Baker, J. Jiang, C. Lagier-Tourenne, D. Edbauer, D. W. Cleveland, R. Rademakers, K. B. Boylan, G. Bu, C. D. Link, C. A. Dickey, J. D. Rothstein, D. W. Dickson, J. D. Fryer, L. Petrucelli, C9ORF72 poly(GA) aggregates sequester and impair HR23 and nucleocytoplasmic transport proteins. *Nat. Neurosci.* **19**, 668–677 (2016).
 45. X. Wen, W. Tan, T. Westergard, K. Krishnamurthy, S. S. Markandiah, Y. Shi, S. Lin, N. A. Shneider, J. Monaghan, U. B. Pandey, P. Pasinelli, J. K. Ichida, D. Trotti, Antisense proline-arginine RAN dipeptides linked to C9ORF72-ALS/FTD form toxic nuclear aggregates that initiate in vitro and in vivo neuronal death. *Neuron* **84**, 1213–1225 (2014).
 46. L. McGurk, E. Gomes, L. Guo, J. Shorter, N. M. Bonini, Poly(ADP-ribose) engages the TDP-43 nuclear-localization sequence to regulate granulo-filamentous aggregation. *Biochemistry* **57**, 6923–6926 (2018).
 47. L. McGurk, E. Gomes, L. Guo, J. Mojsilovic-Petrovic, V. Tran, R. G. Kalb, J. Shorter, N. M. Bonini, Poly(ADP-Ribose) prevents pathological phase separation of TDP-43 by promoting liquid demixing and stress granule localization. *Mol. Cell* **71**, 703–717.e9 (2018).
 48. T. I. Kam, X. Mao, H. Park, S. C. Chou, S. S. Karuppagounder, G. E. Umanah, S. P. Yun, S. Brahmachari, N. Panicker, R. Chen, S. A. Andrabi, C. Qi, G. G. Poirier, O. Pletnikova, J. C. Troncoso, L. M. Bekris, J. B. Leverenz, A. Pantelyat, H. S. Ko, L. S. Rosenthal, T. M. Dawson, V. L. Dawson, Poly(ADP-ribose) drives pathologic α -synuclein neurodegeneration in Parkinson's disease. *Science* **362**, eaat8407 (2018).
 49. C. A. Vivello, R. Wat, C. Agrawal, H. Y. Tee, A. K. L. Leung, ADPRiBoDB: The database of ADP-ribosylated proteins. *Nucleic Acids Res.* **45**, D204–D209 (2017).
 50. F. Teloni, M. Altmeyer, Readers of poly(ADP-ribose): Designed to be fit for purpose. *Nucleic Acids Res.* **44**, 993–1006 (2016).
 51. M. Altmeyer, K. J. Neelsen, F. Teloni, I. Pozdnyakova, S. Pellegrino, M. Grafte, M.-B. D. Rask, W. Streicher, S. Jungmichel, M. L. Nielsen, J. Lukas, Liquid demixing of intrinsically disordered proteins is seeded by poly(ADP-ribose). *Nat. Commun.* **6**, 8088 (2015).
 52. A. Patel, H. O. Lee, L. Jawerth, S. Maharana, M. Jahnel, M. Y. Hein, S. Stojnov, J. Mahamid, S. Saha, T. M. Franzmann, A. Pozniakovski, I. Poser, N. Maghelli, L. A. Royer, M. Weigert, E. W. Myers, S. Grill, D. Drechsel, A. A. Hyman, S. Alberti, A liquid-to-solid phase transition of the ALS protein FUS accelerated by disease mutation. *Cell* **162**, 1066–1077 (2015).
 53. K. Kawashima, M. Izawa, Poly(ADP-ribose) synthesis in nucleoli and ADP-ribosylation of nucleolar proteins in mouse ascites tumor cells in vitro. *J. Biochem.* **89**, 1889–1901 (1981).
 54. A. K. Leung, S. Vyas, J. E. Rood, A. Bhutkar, P. A. Sharp, P. Chang, Poly(ADP-ribose) regulates stress responses and microRNA activity in the cytoplasm. *Mol. Cell* **42**, 489–499 (2011).
 55. C. Guetg, R. Santoro, Noncoding RNAs link PARP1 to heterochromatin. *Cell Cycle* **11**, 2217–2218 (2012).
 56. M. Dasovich, M. Q. Beckett, S. Bailey, S.-E. Ong, M. M. Greenberg, A. K. L. Leung, Identifying poly(ADP-ribose)-binding proteins with photoaffinity-based proteomics. *J. Am. Chem. Soc.* **133**, 3037–3042 (2011).
 57. D.-S. Kim, C. V. Camacho, A. Nagari, V. S. Malladi, S. Challa, W. L. Kraus, Activation of PARP-1 by snoRNAs controls ribosome biogenesis and cell growth via the RNA helicase DDX21. *Mol. Cell* **75**, 1270–1285.e14 (2019).
 58. Y. Ando, E. Elkayam, R. L. McPherson, M. Dasovich, S.-J. Cheng, J. Voorneveld, D. V. Filippov, S.-E. Ong, L. Joshua-Tor, A. K. L. Leung, ELTA: Enzymatic labeling of terminal ADP-ribose. *Mol. Cell* **73**, 845–856.e5 (2019).
 59. E. B. Van Munster, G. J. Kremers, M. J. W. Adjobo-Hermans, T. W. J. Gadella Jr., Fluorescence resonance energy transfer (FRET) measurement by gradual acceptor photobleaching. *J. Microsc.* **218**(Pt 3), 253–262 (2005).
 60. N. Kedersha, M. D. Panas, C. A. Achorn, S. Lyons, S. Tisdale, T. Hickman, M. Thomas, J. Lieberman, G. McInerney, P. Ivanov, P. Anderson, G3BP-Caprin1-USP10 complexes mediate stress granule condensation and associate with 40S subunits. *J. Cell Biol.* **212**, 845–860 (2016).
 61. V. Ayyappan, R. Wat, C. Barber, C. A. Vivello, K. Gauch, P. Visanpattanasin, G. Cook, C. Sazeides, A. K. L. Leung, ADPRiBoDB 2.0: An updated database of ADP-ribosylated proteins. *Nucleic Acids Res.* **49**, D261–D265 (2020).
 62. S. Saberi, J. E. Stauffer, J. Jiang, S. D. Garcia, A. E. Taylor, D. Schulte, T. Ohkubo, C. L. Schloffman, M. Maldonado, M. Baughn, M. J. Rodriguez, D. Pizzo, D. Cleveland, J. Ravits, Sense-encoded poly-GR dipeptide repeat proteins correlate to neurodegeneration and uniquely co-localize with TDP-43 in dendrites of repeat-expanded C9orf72 amyotrophic lateral sclerosis. *Acta Neuropathol.* **135**, 459–474 (2018).
 63. L. Guo, H. J. Kim, H. Wang, J. Monaghan, F. Freyermuth, J. C. Sung, K. O'Donovan, C. M. Fare, Z. Diaz, N. Singh, Z. C. Zhang, M. Coughlin, E. A. Sweeney, M. E. De Santis, M. E. Jackrel, C. B. Rodell, J. A. Burdick, O. D. King, A. D. Gitler, C. Lagier-Tourenne, U. B. Pandey, Y. M. Chook, J. P. Taylor, J. Shorter, Nuclear-import receptors reverse aberrant phase transitions of RNA-binding proteins with prion-like domains. *Cell* **173**, 677–692.e20 (2018).
 64. S. Hutten, S. Usluer, B. Bourgeois, F. Simonetti, H. M. Odeh, C. M. Fare, M. Czuppa, M. Hruska-Plochan, M. Hofweber, M. Polymenidou, J. Shorter, D. Edbauer, T. Madl, D. Dormann, Nuclear import receptors directly bind to arginine-rich dipeptide repeat proteins and suppress their pathological interactions. *Cell Rep.* **33**, 108538 (2020).
 65. L. D. Goodman, M. Prudencio, A. R. Srinivasan, O. M. Rifai, V. M. Y. Lee, L. Petrucelli, N. M. Bonini, eIF4B and eIF4H mediate GR production from expanded G4C2 in a Drosophila model for C9orf72-associated ALS. *Acta Neuropathol. Commun.* **7**, 62 (2019).
 66. M. Prudencio, P. K. Gonzales, C. N. Cook, T. F. Gendron, L. M. Daugherty, Y. Song, M. T. W. Ebbert, M. van Blitterswijk, Y.-J. Zhang, K. Jansen-West, M. C. Baker, M. De Ture, R. Rademakers, K. B. Boylan, D. W. Dickson, L. Petrucelli, C. D. Link, Repetitive element transcripts are elevated in the brain of C9orf72 ALS/FTLD patients. *Hum. Mol. Genet.* **26**, 3421–3431 (2017).
 67. M. Hasegawa, T. Arai, T. Nonaka, F. Kametani, M. Yoshida, Y. Hashizume, T. G. Beach, E. Buratti, F. Baralle, M. Morita, I. Nakano, T. Oda, K. Tsuchiya, H. Akiyama, Phosphorylated TDP-43 in frontotemporal lobar degeneration and amyotrophic lateral sclerosis. *Ann. Neurol.* **64**, 60–70 (2008).
 68. M. Neumann, L. K. Kwong, E. B. Lee, E. Kremmer, A. Flatley, Y. Xu, M. S. Forman, D. Troost, H. A. Kretzschmar, J. Q. Trojanowski, V. M.-Y. Lee, Phosphorylation of S409/410 of TDP-43 is a consistent feature in all sporadic and familial forms of TDP-43 proteinopathies. *Acta Neuropathol.* **117**, 137–149 (2009).
 69. C. Walker, S. Herranz-Martin, E. Karyka, C. Liao, K. Lewis, W. Elsayed, V. Lukashchuk, S.-C. Chiang, S. Ray, P. J. Mulcahy, M. Jurga, I. Tsagakis, T. Iannitti, J. Chandran, I. Coldicott, K. J. de Vos, M. K. Hassan, A. Higginbottom, P. J. Shaw, G. M. Hautbergue, M. Azzouz, S. F. el-Khamisy, C9orf72 expansion disrupts ATM-mediated chromosomal break repair. *Nat. Neurosci.* **20**, 1225–1235 (2017).
 70. R. Lopez-Gonzalez, Y. Lu, T. F. Gendron, A. Karydas, H. Tran, D. Yang, L. Petrucelli, B. L. Miller, S. Almeida, F.-B. Gao, Poly(GR) in C9ORF72-related ALS/FTD compromises mitochondrial function and increases oxidative stress and DNA damage in iPSC-derived motor neurons. *Neuron* **92**, 383–391 (2016).
 71. C. Brochier, J. I. Jones, D. E. Willis, B. Langley, Poly(ADP-ribose) polymerase 1 is a novel target to promote axonal regeneration. *Proc. Natl. Acad. Sci. U.S.A.* **112**, 15220–15225 (2015).
 72. V. Sorrentino, M. Romani, L. Mouchiroud, J. S. Beck, H. Zhang, D. D'Amico, N. Moullan, F. Potenza, A. W. Schmid, S. Rietsch, S. E. Counts, J. Auwerx, Enhancing mitochondrial proteostasis reduces amyloid- β proteotoxicity. *Nature* **552**, 187–193 (2017).
 73. L. A. Becker, B. Huang, G. Bieri, R. Ma, D. A. Knowles, P. Jafar-Nejad, J. Messing, H. J. Kim, A. Soriano, G. Auburger, S. M. Pulst, J. P. Taylor, F. Rigo, A. D. Gitler, Therapeutic reduction of ataxin-2 extends lifespan and reduces pathology in TDP-43 mice. *Nature* **544**, 367–371 (2017).
 74. D. J. Apicco, P. E. A. Ash, B. Maziuk, C. L. Blang, M. Medalla, A. A. Abdullatif, A. Ferragud, E. Botelho, H. I. Ballance, U. Dhawan, S. Boudeau, A. L. Cruz, D. Kashy, A. Wong, L. R. Goldberg, N. Yazdani, C. Zhang, C. Y. Ung, Y. Tripodis, N. M. Kanaan, T. Ikezu, P. Cottone, J. Leszyk, H. Li, J. Luebke, C. D. Bryant, B. Wolozin, Reducing the RNA binding protein TIA1 protects against tau-mediated neurodegeneration in vivo. *Nat. Neurosci.* **21**, 72–80 (2018).
 75. A. C. Elden, H.-J. Kim, M. P. Hart, A. S. Chen-Plotkin, B. S. Johnson, X. Fang, M. Armakola, F. Geser, R. Greene, M. M. Lu, A. Padmanabhan, D. Clay-Falcone, L. McCluskey, L. Elman, D. Juhr, P. J. Gruber, U. Rüb, G. Auburger, J. Q. Trojanowski, V. M.-Y. Lee, V. M. van Deerlin, N. M. Bonini, A. D. Gitler, Ataxin-2 intermediate-length polyglutamine expansions are associated with increased risk for ALS. *Nature* **466**, 1069–1075 (2010).
 76. H. J. Kim, A. R. Raphael, E. S. LaDow, L. McGurk, R. A. Weber, J. Q. Trojanowski, V. M.-Y. Lee, S. Finkbeiner, A. D. Gitler, N. M. Bonini, Therapeutic modulation of eIF2 α phosphorylation rescues TDP-43 toxicity in amyotrophic lateral sclerosis disease models. *Nat. Genet.* **46**, 152–160 (2014).
 77. M. Halliday, H. Radford, Y. Sekine, J. Moreno, N. Verity, J. le Quesne, C. A. Ortori, D. A. Barrett, C. Fromont, P. M. Fischer, H. P. Harding, D. Ron, G. R. Mallucci, Partial restoration of protein synthesis rates by the small molecule ISRIB prevents neurodegeneration without pancreatic toxicity. *Cell Death Dis.* **6**, e1672 (2015).
 78. Y. L. Wong, L. L. Bon, A. M. Basso, K. L. Kohlhaas, A. L. Nikkel, H. M. Robb, D. L. Donnelly-Roberts, J. Prakash, A. M. Swensen, N. D. Rubinstein, S. Krishnan, F. E. McAllister, N. V. Haste,

- J. O'Brien, M. Roy, A. Ireland, J. M. Frost, L. Shi, S. Riedmaier, K. Martin, M. J. Dart, C. Sidrauski, eIF2B activator prevents neurological defects caused by a chronic integrated stress response. *eLife* **8**, e42940 (2019).
79. J. Chew, T. F. Gendron, M. Prudencio, H. Sasaguri, Y.-J. Zhang, M. Castanedes-Casey, C. W. Lee, K. Jansen-West, A. Kurti, M. E. Murray, K. F. Bieniek, P. O. Bauer, E. C. Whitelaw, L. Rousseau, J. N. Stankowski, C. Stetler, L. M. Daugherty, E. A. Perkerson, P. Desaro, A. Johnston, K. Overstreet, D. Edbauer, R. Rademakers, K. B. Boylan, D. W. Dickson, J. D. Fryer, L. Petrucelli, *C9ORF72* repeat expansions in mice cause TDP-43 pathology, neuronal loss, and behavioral deficits. *Science* **348**, 1151–1154 (2015).
80. E. K. Boamah, E. Kotova, M. Garabedian, M. Jarnik, A. V. Tulin, Poly(ADP-Ribose) polymerase 1 (PARP-1) regulates ribosomal biogenesis in *Drosophila* nucleoli. *PLoS Genet.* **8**, e1002442 (2012).
81. G. P. Ritson, S. K. Custer, B. D. Freibaum, J. B. Guinto, D. Geffel, J. Moore, W. Tang, M. J. Winton, M. Neumann, J. Q. Trojanowski, V. M. Y. Lee, M. S. Forman, J. P. Taylor, TDP-43 mediates degeneration in a novel *Drosophila* model of disease caused by mutations in *VCP/p97*. *J. Neurosci.* **30**, 7729–7739 (2010).
82. N. A. Ababneh, J. Scaber, R. Flynn, A. Douglas, P. Barbagallo, A. Candalija, M. R. Turner, D. Sims, R. Dafinca, S. A. Cowley, K. Talbot, Correction of amyotrophic lateral sclerosis related phenotypes in induced pluripotent stem cell-derived motor neurons carrying a hexanucleotide expansion mutation in *C9orf72* by CRISPR/Cas9 genome editing using homology-directed repair. *Hum. Mol. Genet.* **29**, 2200–2217 (2020).
83. J. C. Ame, A. Hakmé, D. Quenet, E. Fouquierel, F. Dantzer, V. Schreiber, Detection of the nuclear poly(ADP-ribose)-metabolizing enzymes and activities in response to DNA damage. *Methods Mol. Biol.* **464**, 267–283 (2009).
84. J. Bischof, R. K. Maeda, M. Hediger, F. Karch, K. Basler, An optimized transgenesis system for *Drosophila* using germ-line-specific phiC31 integrases. *Proc. Natl. Acad. Sci. U.S.A.* **104**, 3312–3317 (2007).
85. T. F. Gendron, M. van Blitterswijk, K. F. Bieniek, L. M. Daugherty, J. Jiang, B. K. Rush, O. Pedraza, J. A. Lucas, M. E. Murray, P. Desaro, A. Robertson, K. Overstreet, C. S. Thomas, J. E. Crook, M. Castanedes-Casey, L. Rousseau, K. A. Josephs, J. E. Parisi, D. S. Knopman, R. C. Petersen, B. F. Boeve, N. R. Graff-Radford, R. Rademakers, C. Lagier-Tourenne, D. Edbauer, D. W. Cleveland, D. W. Dickson, L. Petrucelli, K. B. Boylan, Cerebellar *c9RAN* proteins associate with clinical and neuropathological characteristics of *C9ORF72* repeat expansion carriers. *Acta Neuropathol.* **130**, 559–573 (2015).

Acknowledgment: We are grateful to all patients who agreed to donate postmortem tissue. We thank the following individuals or entities for reagents or services: J. Paul Taylor (G3BP1 bacterial expression construct), X. Wen and D. Trotti (DPR-GFP constructs), Bloomington *Drosophila* Stock Center (NIH P400D018537, fly stocks), and R. Cole and the Johns Hopkins mass spectrometry core. **Funding:** This work was funded by the NIH-NINDS/NIA R01NS117461 (to K.Z., Y.-J.Z., and T.F.G.), DoD W81XWH-21-1-0082 (K.Z.), Target ALS (to K.Z., T.E.L., J.D.R., L.G., and T.F.G.), The Frick Foundation for ALS Research (to K.Z. and L.G.), Center for Biomedical Discovery at Mayo Clinic (to K.Z.), NIH R01NS085207 (to J.D.R.), NIH R01NS099320 (to J.D.R.), NIH P01NS099114 (to J.D.R. and T.F.G.), NIH R01NS094239 (to J.D.R.), NIH U24NS078736 (to J.D.R.), Muscular Dystrophy Association (to J.D.R.), ALS Association (to J.D.R. and T.E.L.), Answer ALS (to J.D.R.), The Robert Packard Center for ALS Research (to J.D.R. and T.E.L.), NIH R01NS082563 (to T.E.L.), NIH R01NS094239 (to T.E.L.), NIH P30NS050274 (to T.E.L.), ALS Association (to T.E.L.), RF1NS121143 (to L.G.), Ralph and Marian Falk Medical Research Trust (to L.G.), NIH R01GM104135 (to A.K.L.L.), NIH R37NS067525 (to V.L.D. and T.M.D.), NIH P01NS084974 (to Y.-J.Z. and T.F.G.), NIH R01NS121125 (to T.F.G.), and NIH K99NS123242 (to A.N.C.). **Author contributions:** Conceptualization: K.Z., J.D.R., T.F.G., T.M.D., V.L.D., A.K.L.L., T.E.L., L.G., T.-I.K., E.F., and Y.-J.Z. Methodology: J.G. (fly, iPSN, SG experiments in cells, in vitro analyses, and co-IP), Q.T.M. (SG experiments in cells), A.G. (TDP-43 protein purification), U.S. (pTDP-43 measures in patient tissues), R.P. (fly experiments), B.G.K. (generating PARP1 KO cells), M.D. (PAR synthesis), A.V. (pTDP-43 measures in patient tissue), M.D.H. (*C9ORF72* repeat sequencing), S.L. (PAR synthesis), A.N.C. (iPSN experiments), R.D. (generating isogenic iPSN lines), K.T. (generating isogenic iPSN lines), E.F. (PAR synthesis), D.D. (patient tissue analyses), L.P. (patient tissue analyses), M.v.B. (*C9ORF72* repeat sequencing), L.G. (TDP-43 protein purification), T.F.G. (pTDP-43 measures in patient tissue), and K.Z. [fly, iPSN, SG experiments, in vitro analyses, co-IP, and human tissue analyses for PAR and poly (G.R.)]. Investigation: J.G., M.v.B., T.F.G., and K.Z. Funding acquisition: K.Z., J.D.R., T.E.L., L.G., V.L.D., T.M.D., Y.-J.Z., T.F.G., and A.N.C. Supervision: K.Z., J.D.R., and T.F.G. Writing (original draft): K.Z. and T.F.G. Writing—review and editing: All authors. **Competing interests:** The authors declare that they have no competing interests. **Data and materials availability:** All data are available in the main text or the Supplementary Materials.

Submitted 6 April 2022

Accepted 17 August 2022

Published 14 September 2022

10.1126/scitranslmed.abq3215

Poly(ADP-ribose) promotes toxicity of C9ORF72 arginine-rich dipeptide repeat proteins

Junli GaoQuinlan T. MewborneAmandeep GirdharUdit ShethAlyssa N. CoyneRitika PunathilBong Gu KangMorgan DasovichAustin VeireMariely DeJesus HernandezShuaichen LiuZheng ShiRuxandra DafincaElise FouquereIKevin TalbotTae-In KamYong-Jie ZhangDennis DicksonLeonard PetrucelliMarka van BlitterswijkLin GuoTed M. DawsonValina L. DawsonAnthony K. L. LeungThomas E. LloydTania F. GendronJeffrey D. RothsteinKe Zhang

Sci. Transl. Med., 14 (662), eabq3215. • DOI: 10.1126/scitranslmed.abq3215

Bringing the target up to PAR

The most common genetic form of amyotrophic lateral sclerosis/frontotemporal dementia (ALS/LTD) is caused by repeat expansion of the hexanucleotide GC in the *C9ORF72* gene, the subsequent production of arginine-rich dipeptide repeat proteins (R-DPRs) ultimately resulting in neurodegeneration. Here, Gao *et al.* investigated how R-DPR formation could lead to neuronal loss and showed that the polymer poly(ADP)-ribose (PAR) interacts with R-DPR and promotes stress granule formation and TDP-43 aggregation in fly models. Similar effects were found in samples from patients with ALS/FTD, suggesting that targeting PAR could reduce the deleterious effects of R-DPR in *C9ORF72*-mediated ALS/FTD.

View the article online

<https://www.science.org/doi/10.1126/scitranslmed.abq3215>

Permissions

<https://www.science.org/help/reprints-and-permissions>

Use of this article is subject to the [Terms of service](#)

Science Translational Medicine (ISSN) is published by the American Association for the Advancement of Science, 1200 New York Avenue NW, Washington, DC 20005. The title *Science Translational Medicine* is a registered trademark of AAAS. Copyright © 2022 The Authors, some rights reserved; exclusive licensee American Association for the Advancement of Science. No claim to original U.S. Government Works